A lecture
In The Chalonge School Meudon Workshop 2014 "From Large to Small scale structures in Agreement with Observations: CMB, WDM, Galaxies, Black holes, Neutrinos and Sterile Neutrinos", 2014 June in Paris

ASTRO-H Hunt for Dark Matter

Takayuki TAMURA

ISAS, JAXA, Japan

In collaboration with

- Mitsuda,K., Yamasaki,N., Kamada,A., Yoshida,N., Kitayama, T.
- The ASTRO-H dark matter search group
- Thanks to Matsushita,K., Boyarsky,A., Ruchayskiy, O., Bulbul,E. Takahashi,T. Iizuka,R., Maeda,Y., Sekiya, N.

(1) Introduction: X-ray search for dark matter, Sterile Neutrino, model and past observations

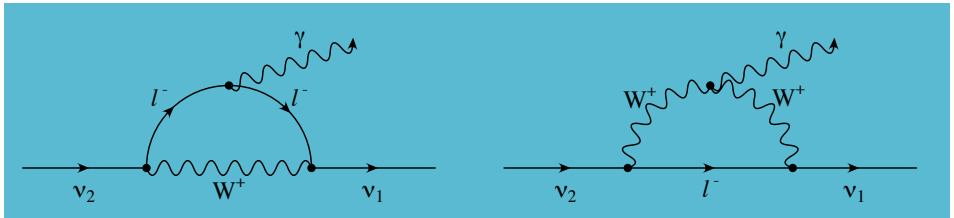

FIG. 2.—Principal radiative decay modes for massive singlet neutrinos

In the past…

(3) *ASTRO-H* Observatory

To be launched in 2015…

(2) *Suzaku* X-ray search for unidentified lines

In this month…

(4) *ASTRO-H* Observation Prospects

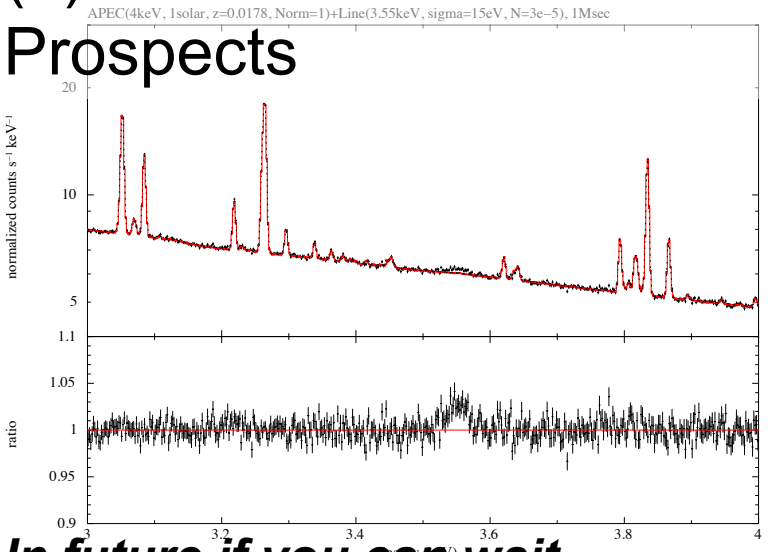

In future if you can wait…

Part-1
X-ray search for dark matter

What is sterile neutrino ?

Past Observations and limits

X-ray signal from dark matter ?

Feng 2010 ARAA, "Dark Matter Candidates from Particle Physics and Methods of Detection"

Table 1 Summary of dark matter particle candidates, their properties, and their potential methods of detection

	WIMPs	SuperWIMPs	Light $\tilde{G}$	Hidden DM	Sterile ν	Axions
Motivation	GHP	GHP	GHP/NPFP	GHP/NPFP	ν Mass	Strong CP
Naturally Correct Ω	Yes	Yes	No	Possible	No	No
Production Mechanism	Freeze Out	Decay	Thermal	Various	Various	Various
Mass Range	GeV-TeV	GeV-TeV	eV-keV	GeV–TeV	keV	μeV–meV
Temperature	Cold	Cold/Warm	Cold/Warm	Cold/Warm	Warm	Cold
Collisional				√		
Early Universe		√√		√		
Direct Detection	√√			√		√√
Indirect Detection	√√	√		√	√√	
Particle Colliders	√√	√√	√√	√		

The particle physics motivations are discussed in Section 2.2; GHP and NPFP are abbreviations for the gauge hierarchy problem and new physics flavor problem, respectively. In the last five rows, √√ denotes detection signals that are generic for this class of dark matter candidate and √ denotes signals that are possible, but not generic. "Early Universe" includes phenomena such as BBN (Big Bang nucleosynthesis) and the CMB (cosmic microwave background); "Direct Detection" implies signatures from dark matter scattering off normal matter in the laboratory; "Indirect Detection" implies signatures of late time dark matter annihilation or decay; and "Particle Colliders" implies signatures of dark matter or its progenitors produced at colliders, such as the Large Hadron Collider (LHC). See the text for details.

(1) Very low interaction → detectable exclusively from cosmic object.
(2) New particles discovered in the earth is the same dark matter in cosmic system ?

THE ASTROPHYSICAL JOURNAL, 562:593–604, 2001 December 1

DIRECT DETECTION OF WARM DARK MATTER IN THE X-RAY

KEVORK ABAZAJIAN,[1] GEORGE M. FULLER,[1] AND WALLACE H. TUCKER[1,2]

Received 2001 May 31; accepted 2001 July 31

ABSTRACT

We point out a serendipitous link between warm dark matter (WDM) models for structure formation on the one hand and the high-sensitivity energy range (1–10 keV) for X-ray photon detection on the *Chandra* and *XMM-Newton* observatories on the other. This fortuitous match may provide either a direct detection of the dark matter or the exclusion of many candidates. We estimate expected X-ray fluxes from field galaxies and clusters of galaxies if the dark matter halos of these objects are composed of WDM candidate particles with rest masses in the structure formation–preferred range ($\sim$1 to $\sim$20 keV) and with small radiative decay branches. Existing observations lead us to conclude that for singlet neutrinos (possessing a very small mixing with active neutrinos) to be a viable WDM candidate they must have rest masses $\lesssim$5 keV in the zero lepton number production mode. Future deeper observations may detect or exclude the entire parameter range for the zero lepton number case, perhaps restricting the viability of singlet neutrino WDM models to those where singlet production is driven by a significant lepton number. The Constellation X project has the capability to detect/exclude singlet neutrino WDM for lepton number values up to 10% of the photon number. We also consider diffuse X-ray background constraints on these scenarios. These same X-ray observations additionally may constrain parameters of active neutrino and gravitino WDM candidates.

Subject headings: dark matter — elementary particles — neutrinos — X-rays: diffuse background — X-rays: galaxies — X-rays: galaxies: clusters

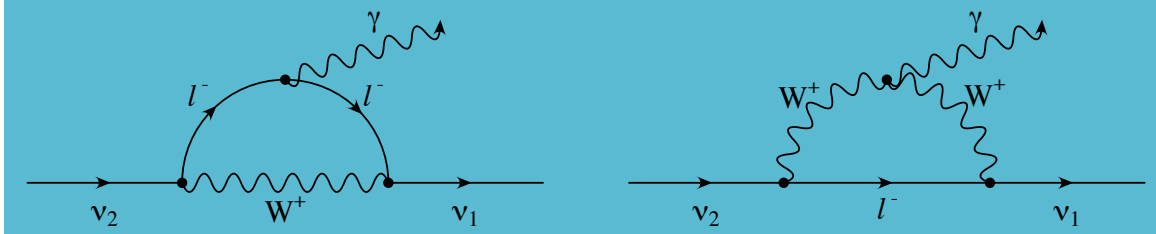

FIG. 2.—Principal radiative decay modes for massive singlet neutrinos

Singlet or sterile neutrino

Here θ is the vacuum mixing angle defined by an *effective* two-by-two unitary transformation between active ν_α species and a singlet species ν_s:

$$|\nu_\alpha\rangle = \cos\theta\,|\nu_1\rangle + \sin\theta\,|\nu_2\rangle\,,$$
$$|\nu_s\rangle = -\sin\theta\,|\nu_1\rangle + \cos\theta\,|\nu_2\rangle\,, \qquad (6)$$

Next decade of sterile neutrino studies

Alexey Boyarsky [a,b,c], Dmytro Iakubovskyi [a,c], Oleg Ruchayskiy [b,d,*]

[a] Instituut-Lorentz for Theoretical Physics, Universiteit Leiden, Niels Bohrweg 2, Leiden, The Netherlands
[b] Ecole Polytechnique Fédérale de Lausanne, FSB/ITP/LPPC, BSP 720, CH-1015 Lausanne, Switzerland
[c] Bogolyubov Institute of Theoretical Physics, Metrologichna str. 14-b, Kyiv, Ukraine
[d] CERN Physics Department, Theory Division, CH-1211 Geneva 23, Switzerland

Dark Universe 1 (2012) 136-

Sterile neutrino is a right-chiral counterpart of the left-chiral neutrinos of the SM ('active'). Adding these particles makes neutrinos massive and provides a simple and natural explanation of the observed neutrino flavor oscillations. These are singlet leptons … they can have a Majorana mass term.

Neutrino Minimal Standard Model (vMSM) aims to explain

(1) neutrino oscillations

(2) baryon asymmetry of the Universe

(3) the existence of dark matter

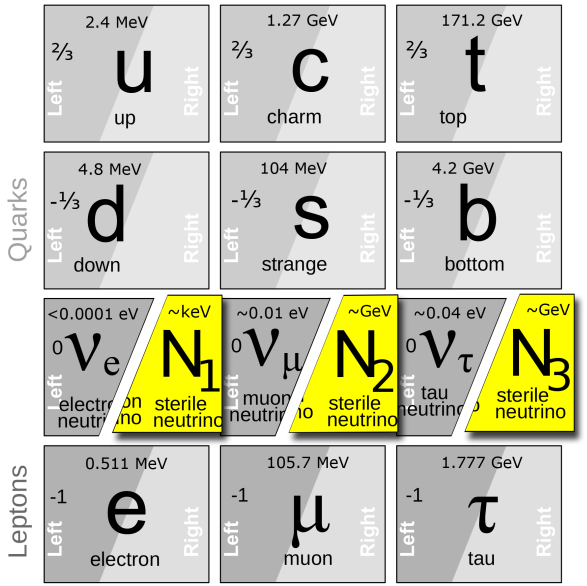

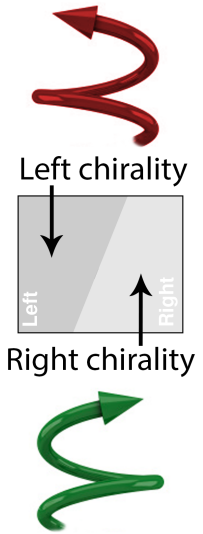

6.2 X-ray flux from Sterile Neutrinos (SN)

Here we give some relations among dark matter parameters and observables given below and in § 5.1.

DM parameters		
DM mass within the fov	$M^{\rm fov}$	$M_\odot$
Luminosity and angular distance	$D_{\rm L}, D_{\rm A}$	pc
Surface mass density (column density)	$\Sigma_{\rm DM}$	$M_\odot$ pc^{-2}
$\nu_{\rm st}$ parameters		
decay rate	Γ	s^{-1}
Mixing angle	2θ	$\sin^2\theta = \frac{1}{4}\sin^2 2\theta$
SN mass	$m_{\rm SN}$	
Instruments/Observables		
X-ray flux from SN	$F_{\rm SN}$	photons cm^{-2} s^{-1}
X-ray flux from SN per solid angle	$f_{\rm SN}$	photons cm^{-2} s^{-1} str^{-1} (LU)

The followings are taken from [Abazajian et al.(2001)] (eq.1, eq.10).

$$L = \frac{E_\gamma}{m_{\rm SN}} M_{\rm DM}\Gamma, \quad (40)$$

$$= 4\pi D_L^2 F \quad (41)$$

$$\Gamma \simeq 6.8\times10^{-33}s^{-1}\left(\frac{\sin^2 2\theta}{10^{-10}}\right)\left(\frac{m_{\rm SN}}{1keV}\right)^5 \quad (42)$$

For the SN decay,

$$E_\gamma = m_{\rm SN}/2. \quad (43)$$

From [Loewenstein & Kusenko(2010)] (eq.2,3)

$$\Gamma \simeq 1.38\times10^{-32}s^{-1}\left(\frac{\sin^2 2\theta}{10^{-10}}\right)\left(\frac{m_{\rm SN}}{1keV}\right)^5 \quad (44)$$

Note that eq. 44 gives two times larger decay rate compared with eq. 42. [3]

$$F_{\rm SN} = 5.15\times\sin^2\theta\times(\frac{m_{SN}}{\rm keV})^4\times M_7^{\rm fov}d_{100}^{-2} \quad (45)$$

$$= 1.3\times10^{-9}\times\sin^2 2\theta\times\left(\frac{m_{SN}}{\rm keV}\right)^4\times(M^{\rm fov}/M_\odot)(D_{\rm L}/Mpc)^{-2}{\rm photons cm^{-2}s^{-1}} \quad (46)$$

$$f_{\rm SN} = \frac{\Sigma_{\rm DM}\Gamma}{4\pi(1+z)^3 m_{\rm SN}} \quad (47)$$

$$\simeq 7.9\times10^{17}\frac{1}{(1+z)^3}(\frac{\Sigma_{\rm DM}}{M_\odot pc^{-2}})(\frac{\Gamma}{\rm s^{-1}})(\frac{m_{\rm SN}}{\rm keV})^{-1}\,{\rm cm^{-2}arcmin^{-2}s^{-1}} \quad (48)$$

$$\simeq 9.3\times10^{-3}\frac{1}{(1+z)^3}(\frac{\Sigma_{\rm DM}}{10^3 M_\odot pc^{-2}})(\frac{\Gamma}{10^{-30}{\rm s^{-1}}})(\frac{m_{\rm SN}}{\rm keV})^{-1}\,{\rm cm^{-2}sr^{-1}s^{-1}}(LU). \quad (49)$$

[3] From ML: On the difference between equations (40) and (42)... Eqn. (40) is for Dirac sterile neutrinos, and Eqn. (42) is for Majorana sterile neutrinos – which picks up the extra factor of two by virtue of it being its own anti-particle. It is generally acknowledged that the latter is more plausible, and that form is usually adopted (including, now, by Abazajian and collaborators).

Past observation targets

Table 2: Proposed and observed targets. R is integrated Radius. Papers: Aba2001; [Abazajian et al.(2001)], Boy2006a; [Boyarsky et al.(2006a)], Boy2008; [Boyarsky et al.(2008)], Boy2010a; [Boyarsky et al.(2010a)], Boy2010b; [Boyarsky et al.(2010b)], L10; [Loewenstein & Kusenko(2010)] L12; [Loewenstein & Kusenko(2012)], M10; [Mirabal(2010)].

paper	Target	D (Mpc)	R (pc)	Mass ($M_\odot$)	Σ ($M_\odot$ pc^{-2})	Ins.
Aba2001	Virgo	2.0e+01	5.6e+04	1.0e+13	1.0e+03	CXO
Aba2001	A85	2.3e+02	6.4e+05	3.5e+14	2.7e+02	CXO
Aba2001	Perseus	7.2e+01	2.0e+05	1.1e+14	8.4e+02	CXO
Aba2001	NGC 3198	1.8e+01	6.7e+04	4.3e+11	3.1e+01	Con-X
Aba2001	NGC 4123	2.2e+01	3.8e+04	7.0e+10	1.5e+01	Con-X
Boy2006a	CL/Coma (core)	98	–	–	—	XMM
Boy2006a	CL/Coma (outer)	98	–	–	—	XMM
Boy2006a	CL/Virgo (core)	20	–	–	—	XMM
Boy2006a	CL/Virgo (outer)	20	–	–	—	XMM
Boy2008	Cl/Bullet(Main)	1530	2.6e6	1.2e15	60	CXO
Boy2008	Cl/Bullet(Sub)	1530	2.8e5	5e13	210	CXO
Boy2008	dSph/Ursa Minor	0.066	270	3.3e7	150	
Boy2010a	M31/Core($r < 10'$)	0.78	2.5e3	(0.4-1.2)e10	200–600	XMM
Boy2010a	M31/Out($r \sim 40'$)	0.78	2e4	1.3e11	100	
Boy2010a	dSph/Fornax	0.138	560		55	
Boy2010a	dSph/Sculptor	0.079	100		150	
Boy2010b	MW/Center($\theta < 10$deg)	–	–	–	100–1000	Int/SPI
Boy2010b	MW/Core($\theta < 30$deg)	–	–	–	100-200	
Boy2010b	MW/Off($\theta > 90$deg)	–	–	–	50-80	
L09	dSph/Ursa Minor	0.069	400	(6^{+12}_{-3})e7	120	Suzaku
L10	Willman-I	0.038	55	2.6e6	210	CXO/AC
L12	ucd/Willman-I	0.038	100	4.2e6	135	CXO/AC
M10	ucd/Segue-1	0.023	67	6e5	43	Swift
Bul2014	Perseus	72	2.5e+5	1.49e14	76	EPIC
	Coma/Cen/Oph	~ 100	(2-4)e+5	(0.6-4.14)e14	60-80	EPIC
	'other CL'	z=0.1-0.4	-	-	-	EPIC
Boy2014	Perseus	72	2.5e+5	1.49e14	76	EPIC
	M31	0.78	-	-	-	EPIC

Current limit on (Mass vs. mixing angle)

Tremaine-Gunn bound: DM dominated objects should not exceed the density of degenerate Fermi gas.

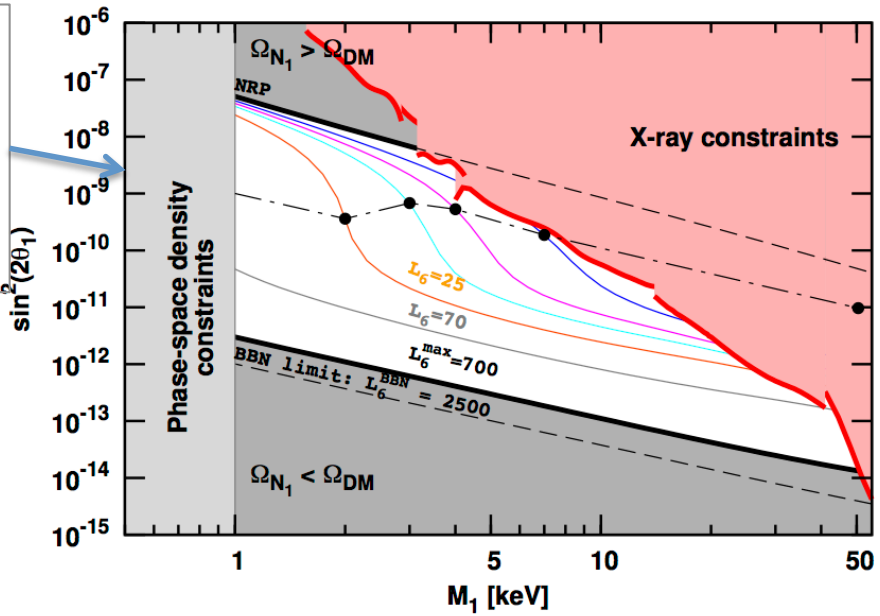

Lines represent production curves for a various types of productions, L_6=10^6(Lepton number)/entropy. NRP: Nonresonance production, L_6=0)

Figure 4: The allowed region of parameters for DM sterile neutrinos produced via mixing with the active neutrinos (*unshaded region*). The two thick black lines bounding this region represent production curves for nonresonant production (NRP) (*upper line*, $L_6 = 0$) and for resonant production (RP) (*lower line*, $L_6^{max} = 700$) with the maximal lepton asymmetry, attainable in the νMSM [53, 48]. The thin colored curves between these lines represent production curves for (*from top to bottom*) $L_6 = 8, 12, 16, 25$, and 70. The red shaded region in the upper right corner represents X-ray constraints [77, 78, 80, 88, 89] (rescaled by a factor of two to account for possible systematic uncertainties in the determination of DM content [86, 80]). The black dashed-dotted line approximately shows the RP models with minimal $\langle q \rangle$ for each mass, i.e., the family of models with the largest cold component. The black filled circles along this line are compatible with the Lyman-α bounds [90], and the points with $M_1 \leq 4$ keV are also compatible with X-ray bounds. The region below 1 keV is ruled out according to the phase-space density arguments [34]. Abbreviation: BBN, big bang nucleosynthesis.

Boyarsky+ 2009a

Bulbul+2014

(6. Caveats) As intriguing as the dark-matter interpretation of our new line is, we should emphasize the significant systematic uncertainties affecting the line energy and flux in addition to the quoted statistical errors. The line is very weak, with an equivalent width in the full-sample spectra of only ~ 1 eV. Given the CCD energy resolution of ~ 100 eV, this means that our line is a ~ 1% bump above the continuum. This is why an accurate continuum model in the immediate vicinity of the line is extremely important; we could not leave even moderately significant residuals unmodeled. … Disentangling these possibilities is impossible at the present energy resolution and has to wait until the launch of *Astro-H*. The other systematic uncertainties mentioned above also have the low energy resolution as their root cause.

The position and flux of the discussed weak line are inevitably subject to systematical uncertainties. There are two weak instrumental lines (K Kα at 3.31 keV and Ca Kα at 3.69 keV), although formally their centroids are separated by more than 4σ. Additionally, the region below 3 keV is difficult to model precisely, especially at large exposures, due to the presence of the absorption edge and galactic emission. However, although the residuals below 3 keV are similar between the M31 dataset (Fig. 1) and the blank sky dataset (Fig. 3), the line is *not detected* in the latter. Although the count rate at these energies is 4 times larger for M31, the exposure for the blank sky is 16 times larger. This disfavors the interpretation of the line as due to a wiggle in the effective area. The properties of this line are consistent (within uncertainties) with the DM interpretation. To reach a conclusion about its nature, one will need to find more objects that give a detection or where non-observation of the line will put tight constraints on its properties. The forthcoming *Astro-H* mission [34] has sufficient spectral resolution to spectrally resolve the line against other nearby features and

A hint of un-id lines from Galactic Bulge with *Suzaku* (Koyama, Nakajima+ 2014, private comm.)

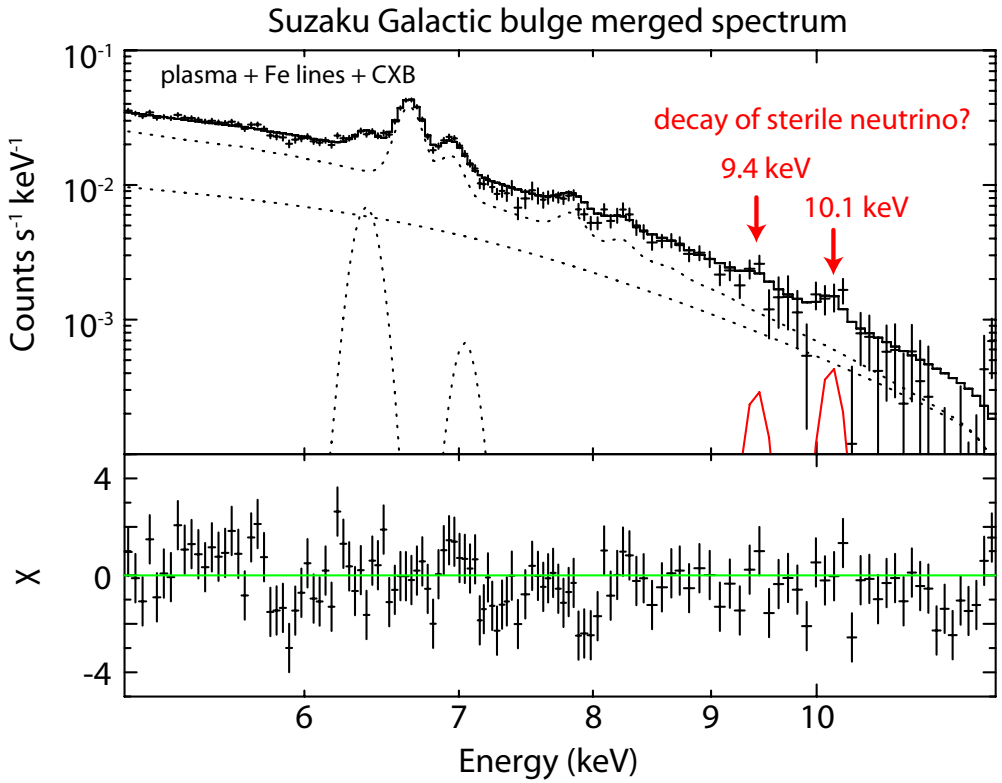

Figure 12: Suzaku spectrum obtained from the Galactic bulge region. Fitting with a CIE model gives line-like residuals at the energies of no atomic line, 9.4 keV and 10.1 keV.

Part-2
Suzaku search for unidentified lines

Can we see the lines with other detectors ?

Origin of unidentified features around 3.5 keV ?

Suzaku (Japan-US X-ray mission 2005~)

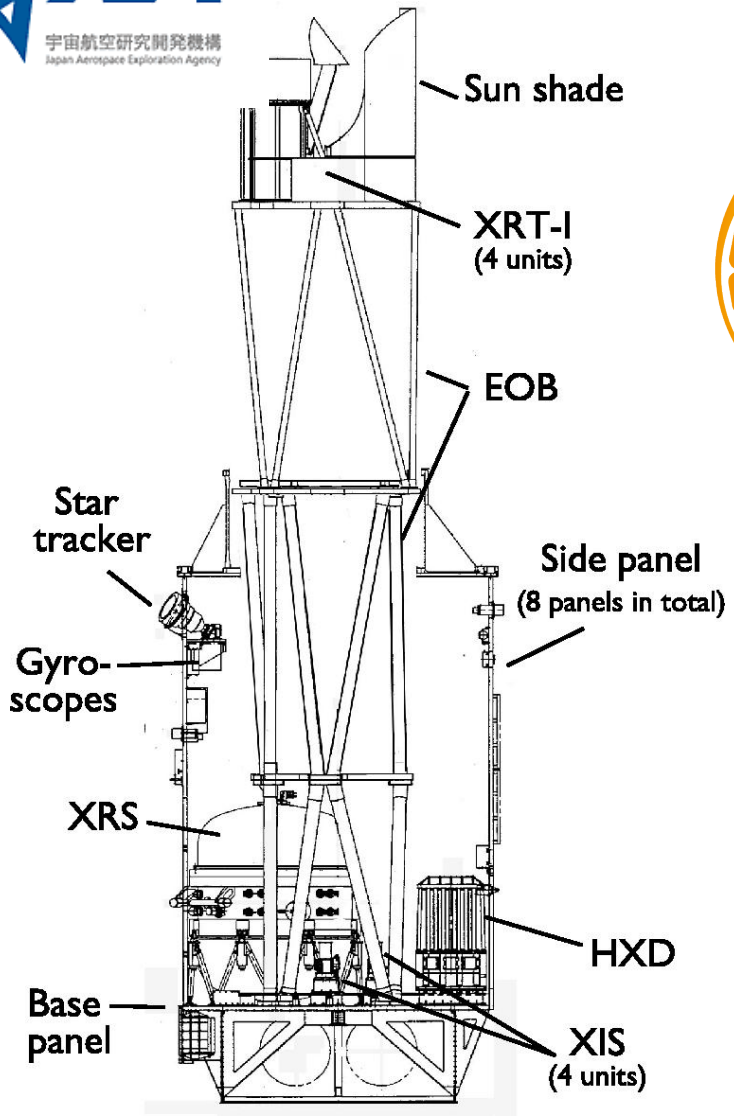

Mitsuda et al. 2007

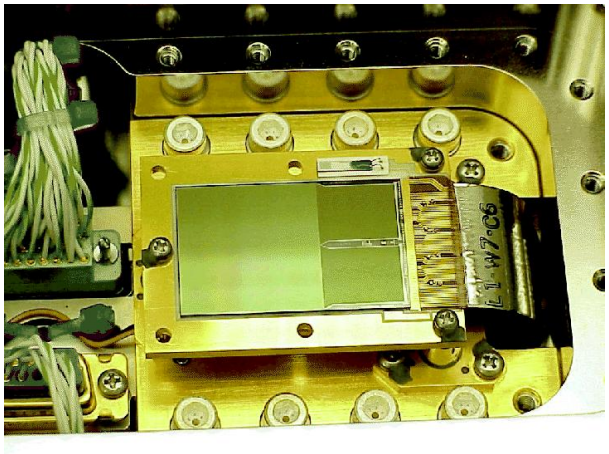

XIS (X-ray Imaging Spectrometer)

- The most-advanced CCD in-orbit.
- Good energy response and calibration.
- Comparable sensitivity, 17'x 17'
- Spatial resolution is ~ 1.5 arcmin.

Suzaku deep and wide observations of the Perseus cluster

Calibration (center) and Key project (large region) target

- 1st detection of X-rays from rare-metals (Mn & Cr), Tamura+ 2009 →
- "Baryons at the Edge of the X-ray-Brightest Galaxy Cluster", Simionescu+ 2011 (Science)
- "A uniform metal distribution in the intergalactic medium of the Perseus cluster of galaxies", Werner+ 2014 (Nature)
- "Gas Bulk Motion in the Perseus Cluster Measured with Suzaku", Tamura+ 2014.

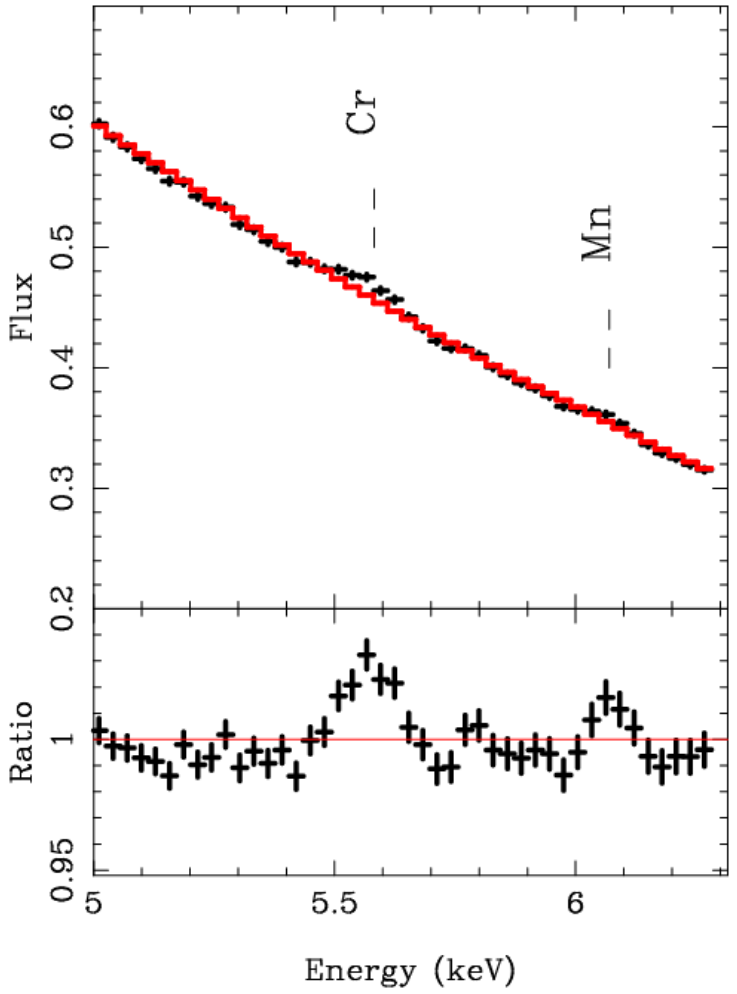

The Perseus *Suzaku* spectra

Total exposure of 655 ks (sum of CCDs)

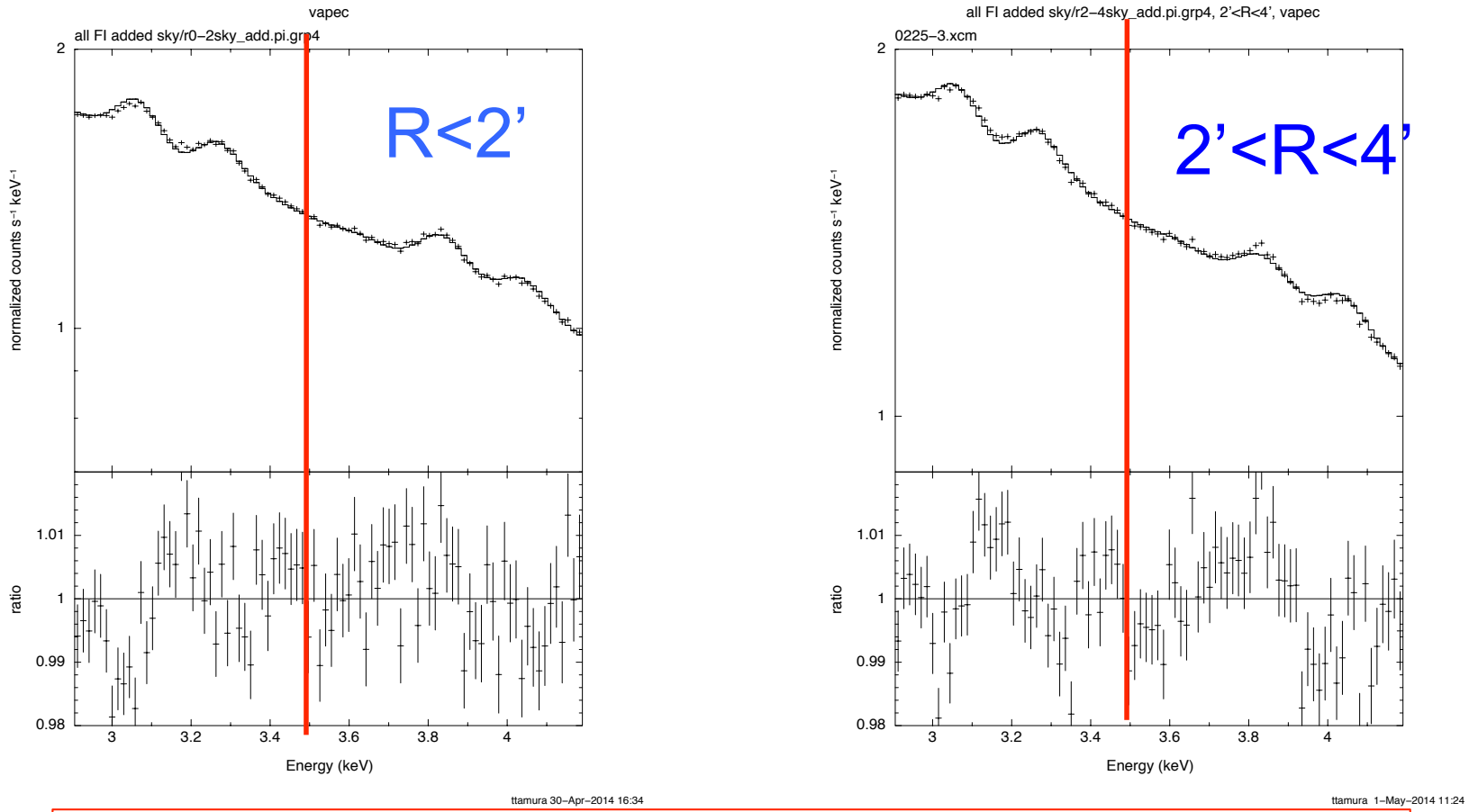

Possible Dark matter line at 3.57± 0.02 keV (rest-frame; Bulbul+, MOS) → 3.51 (observed) keV

Plasma lines (keV) : Ar He-like (3.14), Ar H-like (3.32), Ca He-like(3.90), Ca H-like (4.11).

The Perseus *Suzaku* spectra: R<10’

With the best-fit model. Right panel includes a line with the flux in Bulbul+(2014; 5e-5 cts/sec/cm^2).

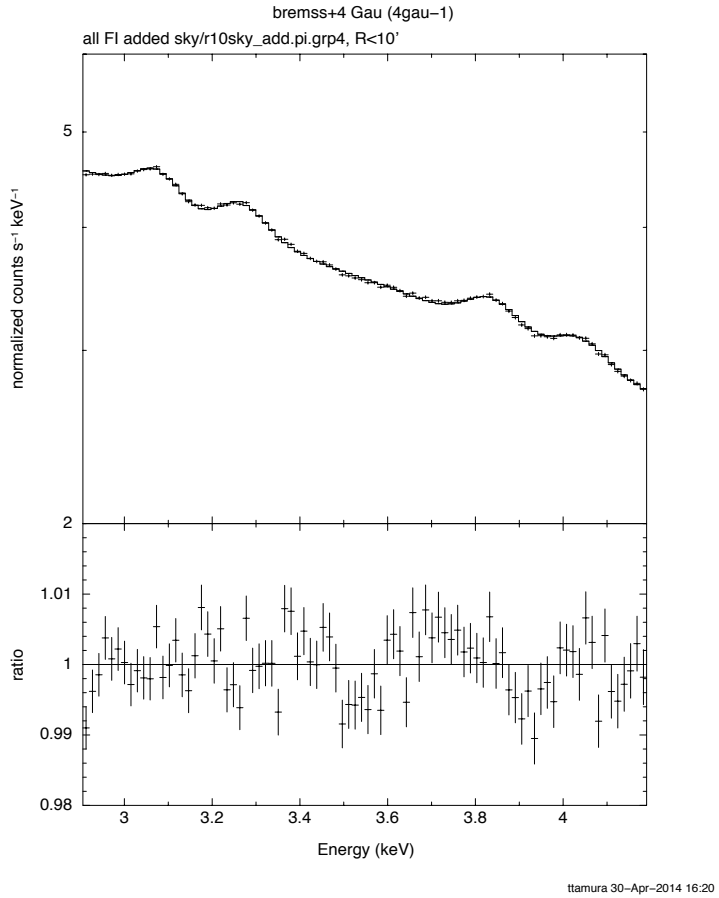

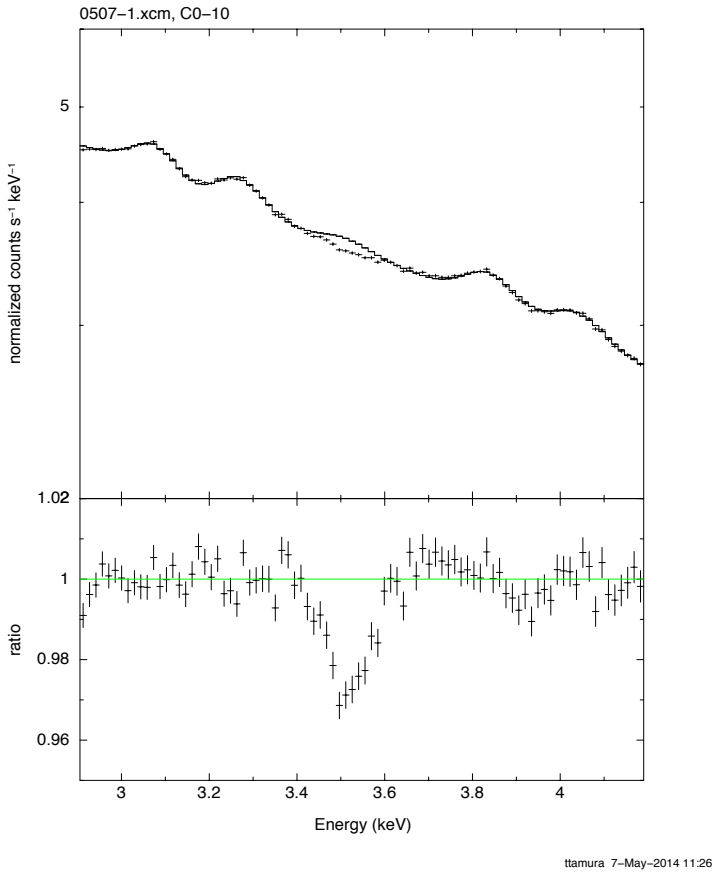

Cr and Mn line detection: R<10’

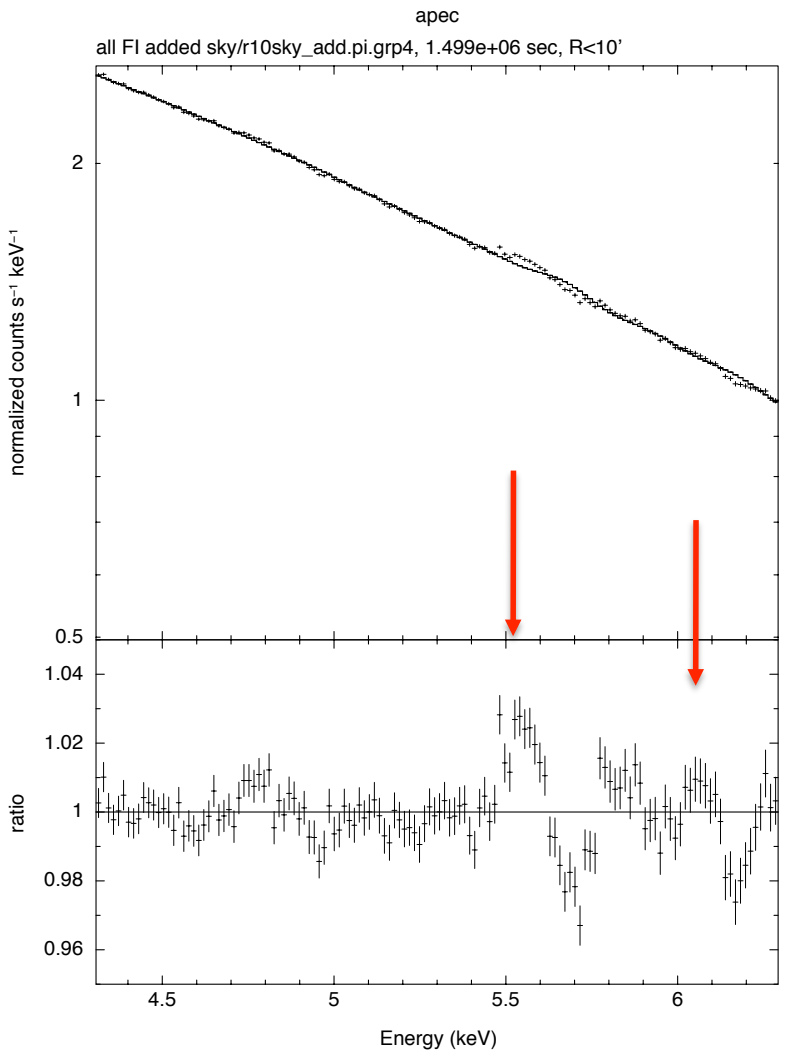

Very weak atomic lines (EW < a few eV) are detected. Cr (5.57keV) & Mn (6.07keV).

Si-escape of He-like Fe at 4.8keV.

The Perseus *Suzaku* spectra: 10'<R<20'

Left→No line, Right→ A line

A weak line could be consistent with the data

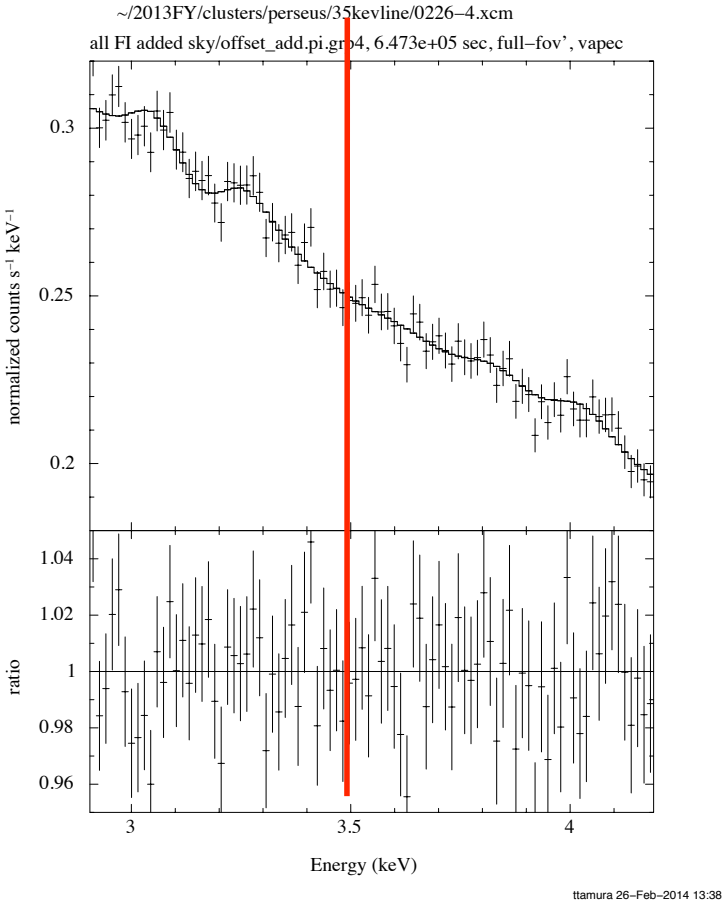

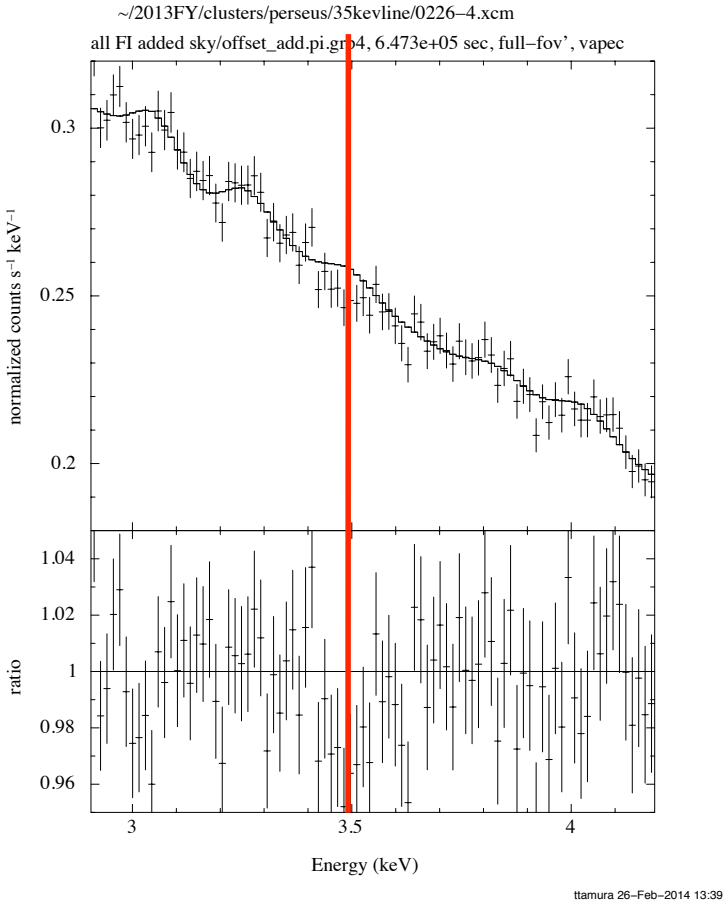

The *Suzaku* Crab spectrum (non-thermal, power-law continuum)

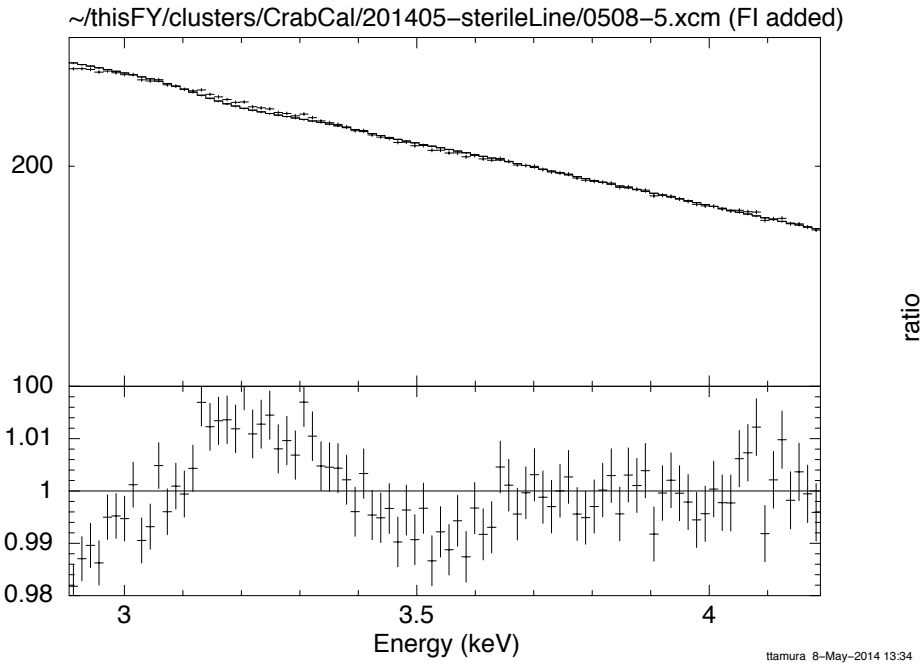

The Crab spectra integrated over observations of the XIS, fitted with a power-law in the 2.9-4.4 keV band.

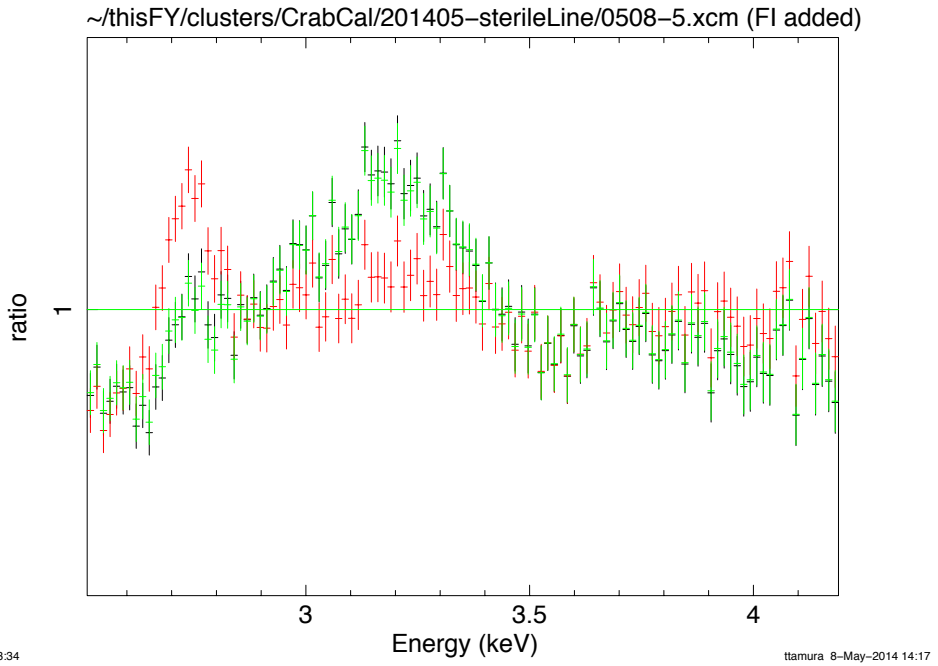

The fit residuals using two different responses. Red are for early phase (~2006) and Green for later phase (~2012).

Systematic residual → Effective area (+energy response) calibration → <2% errors

Au M edges in telescopes (*Suzaku* and XMM telescopes)

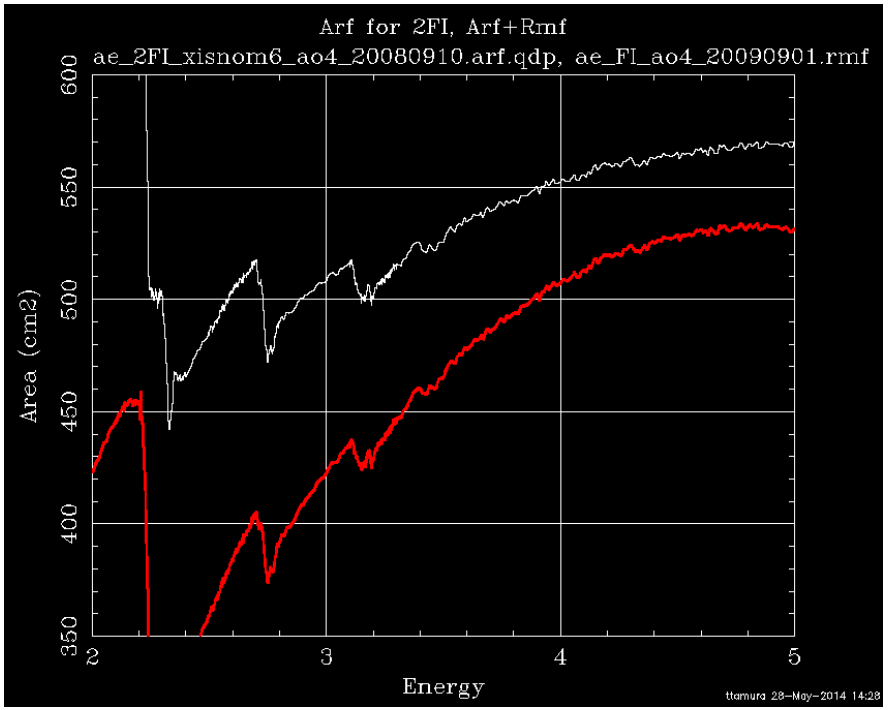

Effective areas of Telescope+CCD and Telescope used in the response.

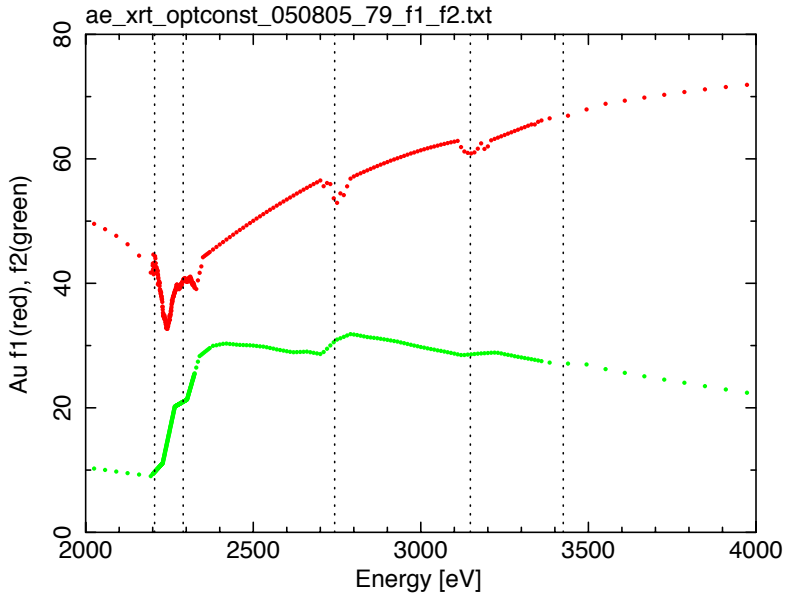

Measurements of Au reflection parameters (f1,f2). These data are used to make Suzaku responses (Iizuka+, priv. comm.). Note that E>3.4keV energy steps becomes coarse.

Suzaku analysis for the 3.5 keV line

- Bulbul et al. (2014) reported detection of an unidentified X-ray line at around 3.5 keV from the Perseus cluster and other clusters with *XMM* EPIC. Boyarsky et al. (2014) reported detection at the same energy from the Perseus cluster and the Andromeda galaxy with EPIC.
- Searching for the 3.5 keV line, we used spectra of the Perseus cluster with *Suzaku* XIS. We used a deep exposure from the cluster center and spectra from larger regions around the center. In both cases, no line has been found so far.
- For the Perseus center data, XMM and Suzaku data are inconsistent with each other. → errors in calibration in either detector.
- One possible origin of miss-calibration → Au M edge fine structure. In X-ray telescopes at least of XMM-Newton and Suzaku , Au is used for reflection coating. The reflection has a small Mu edge around 3.4–3.5 keV.
- → the energy resolution of current detectors (CCDs) is not enough to detect a weak line, identify the origin, separate it any astronomical lines from baryons or instrumental effects.

Part-3 : ASTRO-H

Go to the ASTRO-H Video

And the Quick Reference

Tables and figures from Mitsuda et al. 2010, The High-Resolution X-ray Microcalorimeter Spectrometer System for the SXS on ASTRO-H

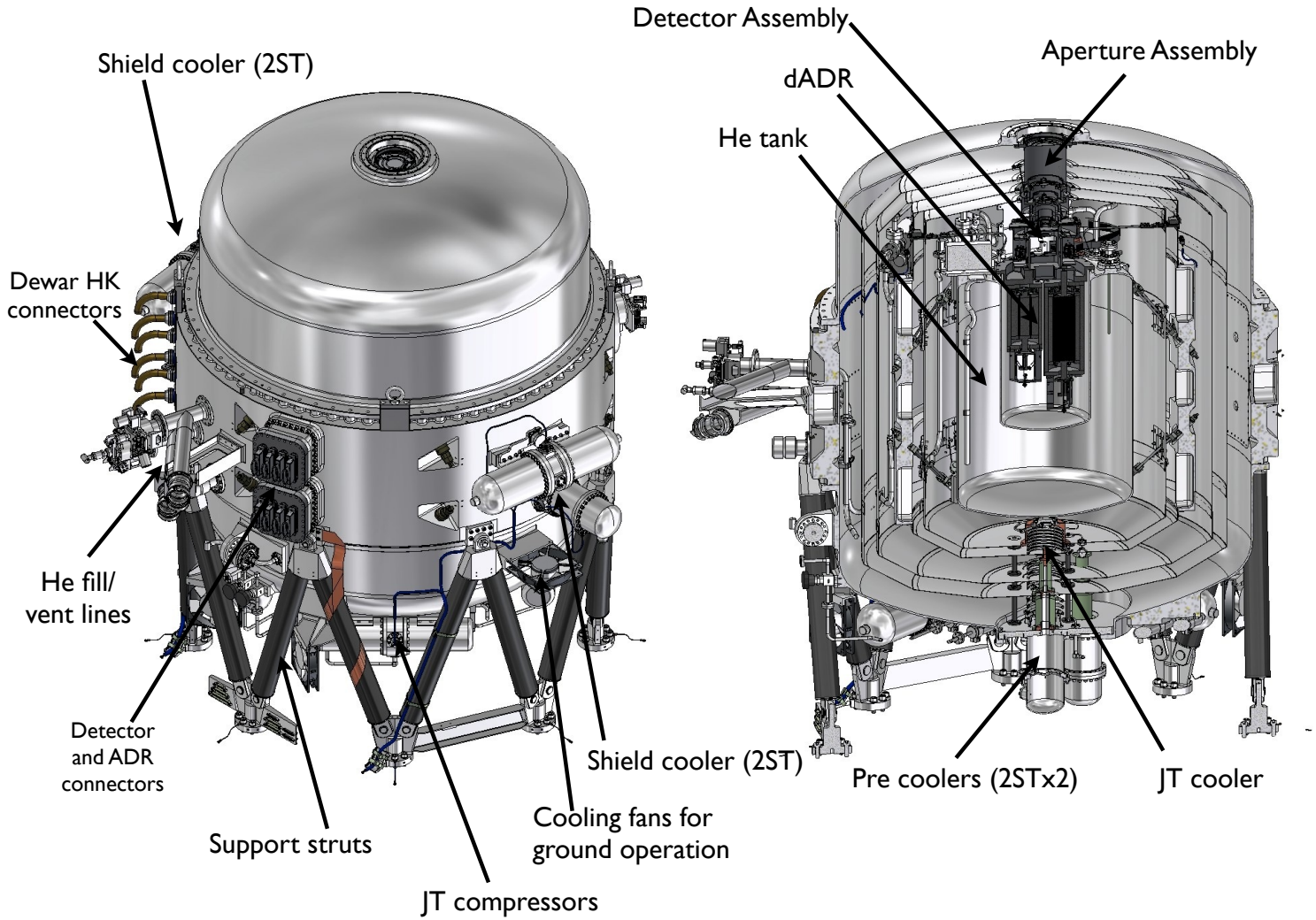

Figure 7. External view (left) and cutaway drawing (right) of the *ASTRO-H* SXS cryogenic Dewar. The gate valve which will be mounted on the top of the Dewar outer shell is not shown. Two shield coolers are mounted on the side of the outer shell, while the JT cooler and its pre coolers are mounted on the bottom. The detector assembly (DA) and the ADR are installed as a unit on the He tank from the upper side. The third ADR is on the side of the DA but is not shown here because it is in the unseen part of the Dewar in the cutaway drawing. The outer diameter of the Dewar outer shell excluding mechanical coolers and other sticking-out structures is 950 mm. The height of the Dewar is 1292 mm including the support struts but excluding the gate valve. The total mass of the Dewar is about 270 kg.

ADR (Adiabatic demagnetization refrigerator)

Table 1. *ASTRO-H* SXS key requirments

	Requirement	Goal
Energy range	0.3 - 12 keV	
Effective area at 1 keV	160 cm^2	
Effective area at 6 keV	210 cm^2	
Energy resolution	7 eV	4 eV
Array format	6×6	
Field of view	$2.9' \times 2.9'$	
Angula resolution	1.7'(HPD)	1.3' (HPD)
Lifetime	3 years	5 years
Time assignment resolution	80 μs	
Maximum counting rate	150 c s^{-1} $pixel^{-1}$	
Energy-scale calibration accuracy	2 eV	1 eV
Line-spread-function calibration accuracy	2 eV	1 eV

Table 2. *ASTRO-H* SXS key design parameters

Parameter	Value
SXS XRT (SXT-S, Thin-foil mirrors)*	
Focal length	5.6 m
Diameter of most outer mirror	45 cm
Reflecting surface	Gold
Thermal shield	Al (300 nm) + PET (0.22 μm) with SUS mesh of a 94 % open fraction
SXS XCS (6×6 microcalorimeter array)	
Operating temperature	50 mK
Pixel size	814 μm $\times$814μm
Pixel pitch	832μm
Field of view	3'.05 $\times$ 3'.05
X-ray absorber	HgTe, 8μm thickness
Optical Blocking filters	5 filters, polyimide (460 nm) + Al (400nm) total, Si mesh on two filters

* See Okajima et al. (2008)[4] for more details of the mirror design.

Effective areas of SXS and other high-resolution X-ray spectrometers

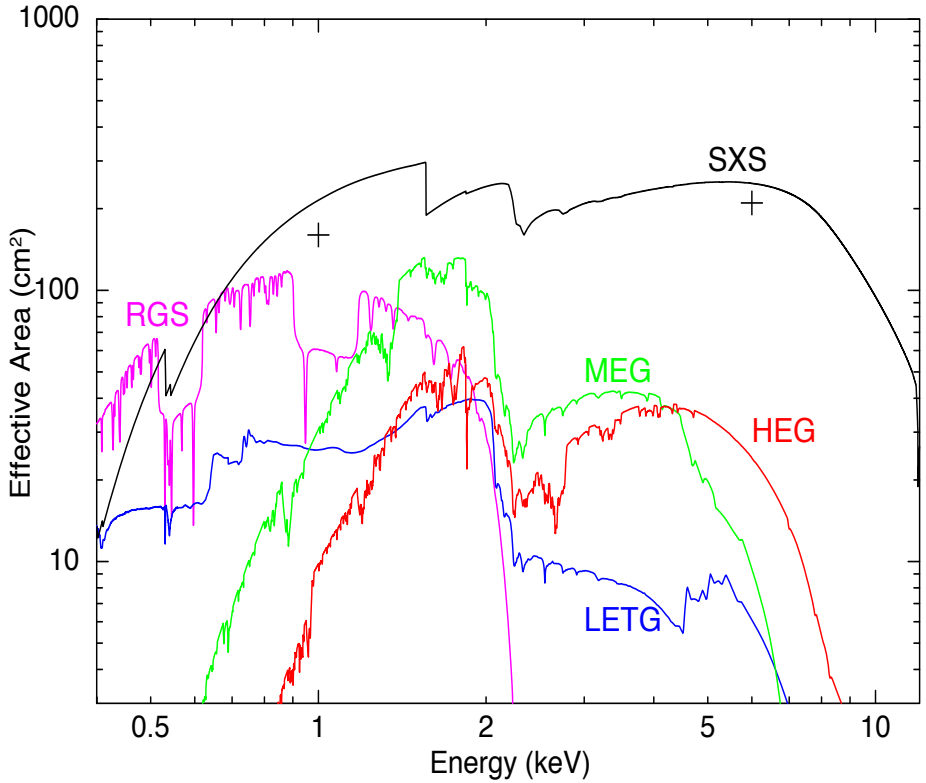

Figure 1. Effective areas of high-resolution X-ray spectroscopy missions as functions of X-ray energy. The curve for the SXS is the present best estimate for a point source, where we assumed to sum all photons detected on the whole array, 1.3' HPD of the X-ray mirrors, and no contamination of the optical blocking filters. The two crosses show the requirements. The RGS effective areas is a sum of first order of the two instruments (RGS-1 and RGS-2), and was derived from the RGS response matrix in SAS v9.0. The effective areas of LETG, MEG and HEG onboard *Chandra* are, respectively, derived from the response files for the cycle 12 proposal, and are a sum of first order dispersions in ± directions. (Color on-line)

Resolving Power of SXS

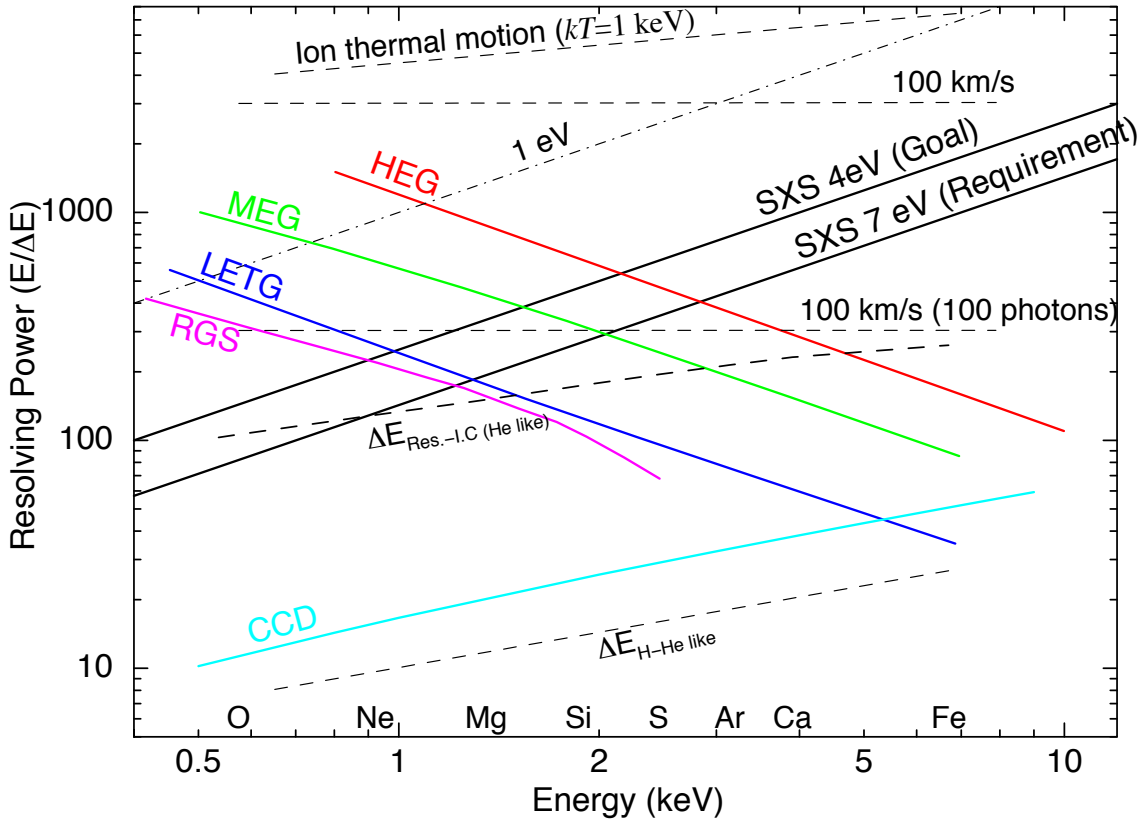

Figure 2. Resolving power of the *ASTRO-H* SXS as a function of X-ray energy for the two cases, 4 eV resolution (goal) and 7 eV (requirment). The resolving power of high resolution instruments on board *Chandra* and *XMM-newton* and typical resolving power of X-ray CCD cameras are also shown for comparison. The typical energy separations between K emission of H-like and He-like ions ($\Delta_{\mathrm{H-Helike}}$) and between resonant and inter combination lines of He-like ions ($\Delta_{\mathrm{Res.-I.C(Helike)}}$) are shown with broken lines, while the emission energies are shown at the bottom of the panel. The broken line denoted with "Ion thermal motion" is the line broadening due to thermal motion of ions in a $kT = 1$ keV plasma. The broken lines indicated with "100 km/s" and "100 km/s (100 photons)" are, respectively, the doppler shift by a bulk motion of the velocity and a typical detection limit with 100 photons in photon-statistics limit, i.e.continuum emission and non X-ray background are negligible. The dot-dash line denoted with "1 eV" shows the line shift/broadening detection limit determined by 1 eV energy-scale or line-spread-function calibration uncertainty. (Color on-line)

An example of high resolution spectroscopy
Galaxy cluster

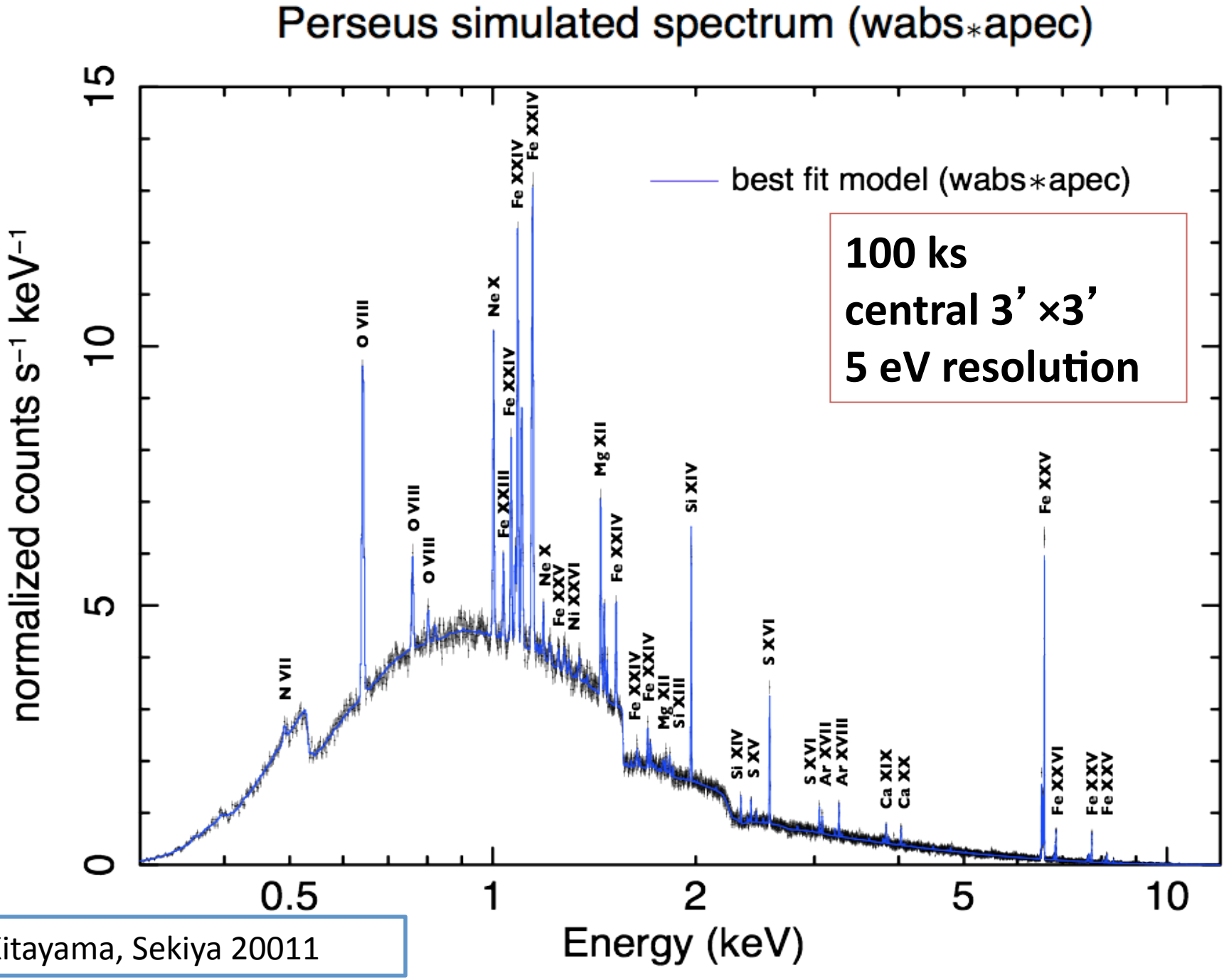

Kitayama, Sekiya 20011

SXS simulation
The brightest cluster core: The Perseus

- Detect and locate the gas turbulence.
- Combined with hard X-ray imaging, gas dynamics, particle acceleration, shocks and non-thermal processes will be investigated.

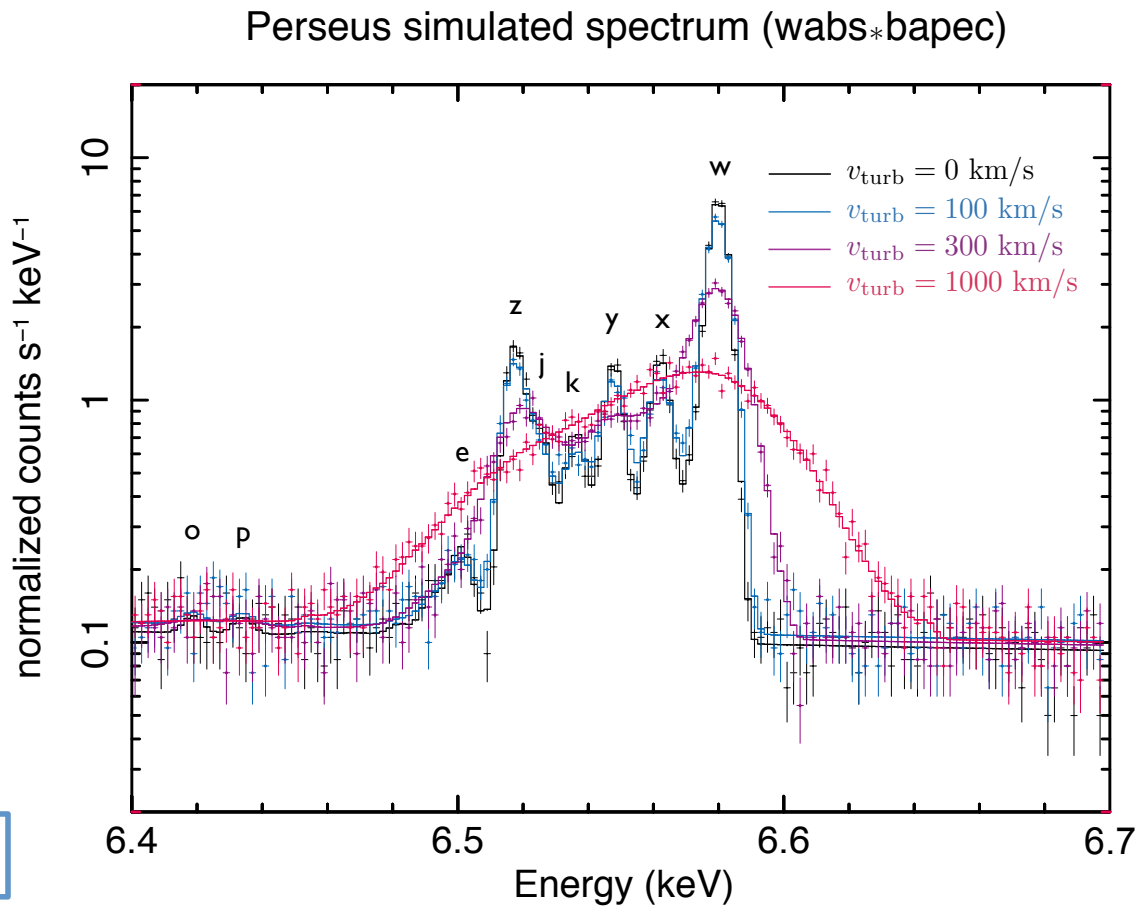

Sekiya 20011

Search for a weak, extended line at unknown energy: AH/SXS or CCDs

- E< 1keV: The soft X-ray diffuse background dominates. Even for SXS, search for a weak line with this line dominated emission would be challenging.
- Some strong instrumental lines in CCD spectra (NXB). Limited energy resolution of CCD makes it difficult to search a line. SXS spectra could be much clean.
- Other bands:
  - Smaller extent source: SXS could be better, depending on DM distribution. Photon limit: T^{-1}.
  - Larger one: Large FOV CCDs could be better. Background limit $T^{-1/2}$
- If a line is detected: SXS can tell precise energy, making it easy to separate from non-DM origins. CCD detection is difficult to exclude non-DM possibilities.

ASTRO-H（2015年，打ち上げ予定）

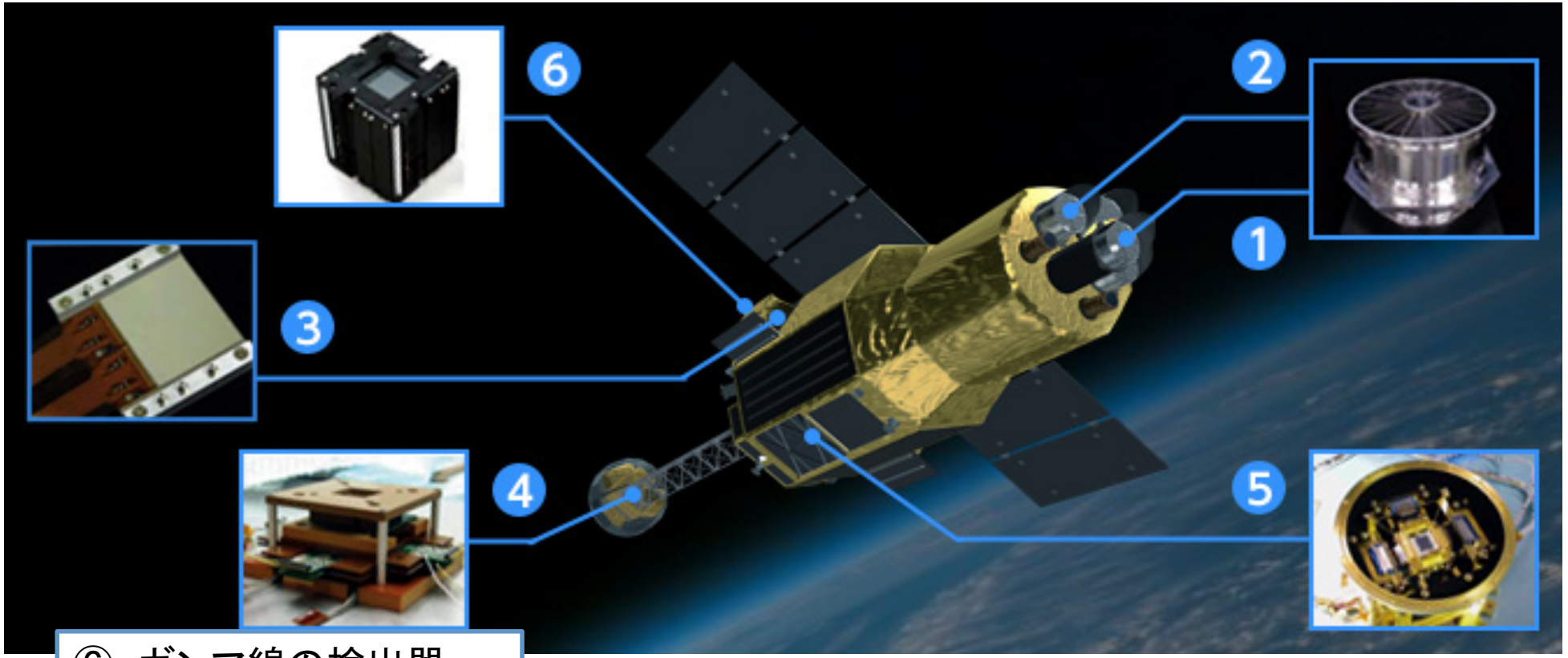

⑥ ガンマ線の検出器 (SGD)

③ X線のCCDカメラ (XIS)

①，② X線を集める望遠鏡 (SXT, HXT)

④ 高エネルギーのX線の検出器

⑤ X線のエネルギーを精密に測る検出器 (SXS)

ASTRO-H instruments

(from AH Quick Reference)

Table 2 *Properties of ASTRO-H instruments (current best estimate)*

Properties	SXS	SXI	HXI	SGD (photo-abs)	SGD (Compton)
Effective area (cm^2)	50/225 (@0.5/6 keV)	214/360 (@0.5/6 keV)	300 (@30 keV)	200 (@30 keV)	30 (@100 keV)
Energy range (keV)	0.3-12.0	0.4-12.0	5-80	10-600	10-600
Angular resolution in HPD (arcmin)	1.3	1.3	1.7	N/A	N/A
Field of view ($arcmin^2$)	3.05x3.05	38x38	9x9	0.55x0.55 (<150 keV)	0.55x0.55 (<150 keV)
Energy resolution in FWHM (eV)	5	150 (@6 keV)	< 2000 (@60 keV)	2000 (@40 keV)	2000 (@40 keV)
Timing resolution (s)	$8x10^{-5}$	4	several x 10^{-5}	several x 10^{-5}	several x 10^{-5}
Instrumental background (/s/keV/FoV)	$2x10^{-3}/0.7x10^{-3}$ (@0.5/6 keV)	0.1/0.1 (@0.5/6 keV)	$6x10^{-3}/2x10^{-4}$ (@10/50 keV)[1] $2x10^{-3}/4x10^{-5}$ (@10/50 keV)[2]		$1x10^{-4}/1x10^{-5}$ (@40/600 keV)

[1]4 layers, [2]1 layer

Part-4
ASTRO-H Observation Prospects

Can *ASTRO-H* detect a signal ?

Can we improve sensitivity and limit ?

What is the best targets for *ASTRO-H* ?

Analytical Estimates of Line Sensitivity

2.1 General case

See for example Yoshikawa et al. (2003) or Mitsuda et al. (deLuxs paper) for similar considerations.

X-ray line flux	$F_{\rm Line}$	photons cm^{-2} s^{-1}
X-ray line flux density	$f_{\rm Line}$	photons cm^{-2} s^{-1} str^{-1} = (Line Unit)
Background flux	$f_{\rm B}$	photons cm^{-2} s^{-1} keV^{-1} str^{-1}
Solid Angle	Ω	str (arcmin^2 = 8.46 $\times$ 10^{-8} str)
Detector effective Area	S	cm^2
Exposure time	T	sec
Energy resolution	ΔE	keV

Detected photon numbers for the source ($C_{\rm Line}$) and background ($C_{\rm B}$):

$$C_{\rm Line} = F_{\rm Line} ST = f_{\rm Line} \Omega S T \quad (1)$$
$$C_{\rm B} = f_{\rm B} \Omega S T \times \Delta E \quad (2)$$

Her we assume that all photons are within ΔE. The signal to noise ratio, S/N, is expected to be,

$$C_{\rm Line} = (C_{\rm Line} + C_{\rm B}) - C_{\rm B} \quad (3)$$
$$(S/N)^2 = \frac{C_{\rm Line}^2}{C_{\rm Line} + 2C_{\rm B}} \quad (4)$$

Here we do not consider systematic errors.

Background could include cosmic, instrumental (NXB), and continuum flux from the source.

$$f_{\rm B} = f_{\rm CXB} + f_{\rm NXB} + f_{\rm source} \quad (5)$$

2.1.1 Fain source, low energy resolution, high background (background limit)

When $C_{\rm Line} \ll C_{\rm B}$, or line equivalent width $EW \ll \Delta E$,

$$(S/N)^2 \simeq \frac{C_{\rm Line}^2}{2C_{\rm B}}$$
$$(S/N) = F_{\rm Line} \left(\frac{ST}{2 f_{\rm B} \Delta E \Omega} \right)^{1/2} \quad (6)$$
$$= f_{\rm Line} \left(\frac{S\Omega T}{2 f_{\rm B} \Delta E} \right)^{1/2} \quad (7)$$

From the above relation, the 3σ limit can be derived as,

$$f_{\rm Line}^{3\sigma,{\rm bgd}} = 3 \times \left(\frac{2 f_{\rm B} \Delta E}{S\Omega T} \right)^{1/2} \quad (8)$$
$$F_{\rm Line}^{3\sigma,{\rm bgd}} \propto f_{\rm Line}^{3\sigma,{\rm bgd}} \Omega = 3 \times \left(\frac{2 f_{\rm B} \Delta E}{ST} \right)^{1/2} \Omega^{1/2} \quad (9)$$

37

2.1.2 Bright source, high energy resolution, low background (photon limit)

When $C_{\rm Line} \gg C_{\rm B}$, or $EW \gg \Delta E$,

$$(S/N)^2 \simeq \frac{C_{\rm Line}^2}{C_{\rm Line}} \quad (10)$$
$$(S/N) \simeq C_{\rm Line}^{1/2} \quad (11)$$
$$= (F_{\rm Line} ST)^{1/2} \quad (12)$$
$$= (f_{\rm Line} S\Omega T)^{1/2} \quad (13)$$

similarly above, the 3σ limit can be derived as,

$$3 = (f_{\rm Line}^{3\sigma,{\rm photon}} S\Omega T)^{1/2} \quad (14)$$
$$f_{\rm Line}^{3\sigma,{\rm photon}} = 9 (S\Omega T)^{-1} \quad (15)$$
$$F_{\rm Line}^{3\sigma,{\rm photon}} = 9 (ST)^{-1} \quad (16)$$

In this case, the S/N is independent of ΔE and limited by the source count statistics.

2.1.3 Need for Monte Carlo simulation with instrumental responses.

Here we should note what ΔE is used. For example, if the line spread function (LSF) is an Gaussian, within the FWHM of the LSF (2.35σ), only about 70% of the source flux is collected. If we want to collect 99% of the flux, we need integrated an energy band within $\pm 2.6\sigma$, which corresponds to 2.2 FWHM. In this case we may use 2.2 FWHM for ΔE [1]. This estimation may be too simple to calculate correct statistics. We may need Monte Carlo simulation of instruments. We may also need to take care for any systematic uncertainty in $f_{\rm B}$.

[1] Note that $1/\sqrt{(2.2)} \sim 0.7$

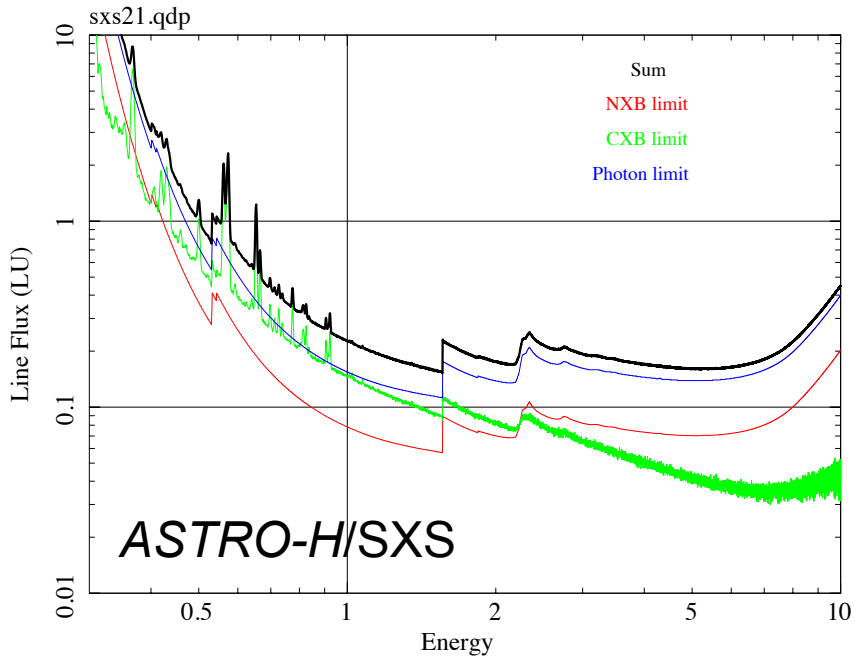

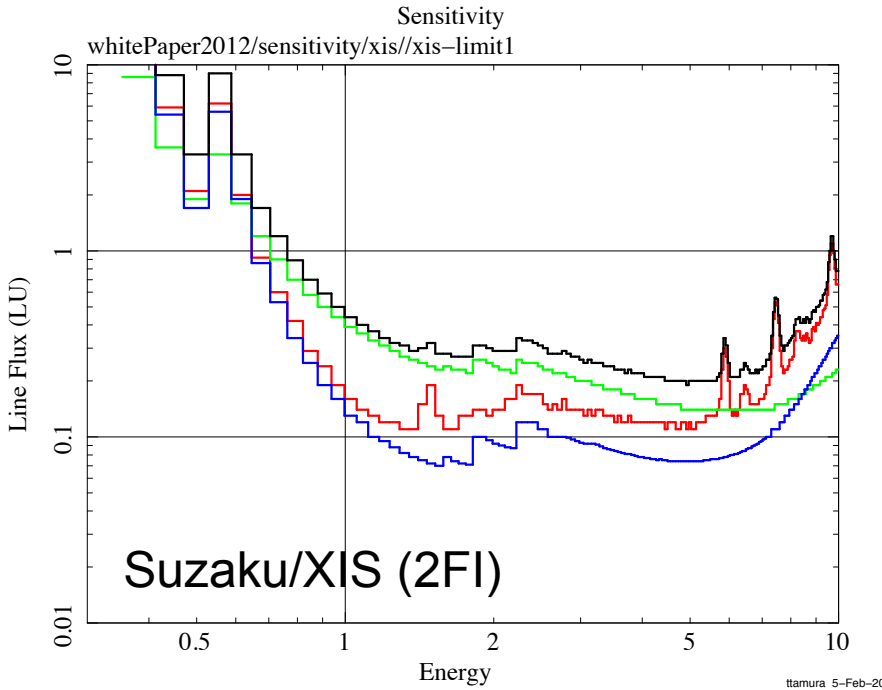

Analytical limit for 3 sigma detection.
Ω = 9 arcmin2 and 300 ksec

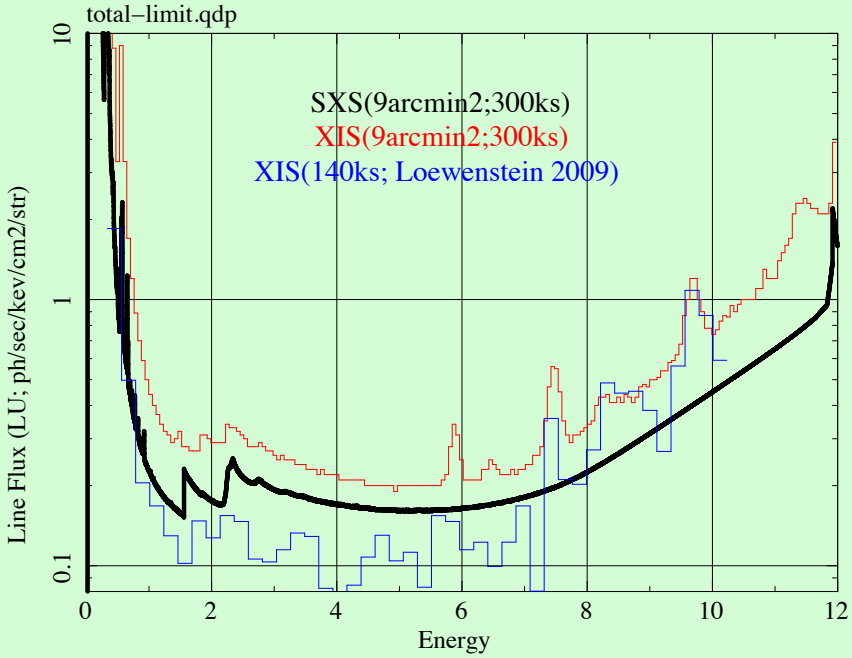

Blue line from Monte-Carlo simulation by Loewenstein+2009 with larger Ω.

ASTRO-H/SXS+Σ_{DM}=500 $M_\odot/pc^2$ source

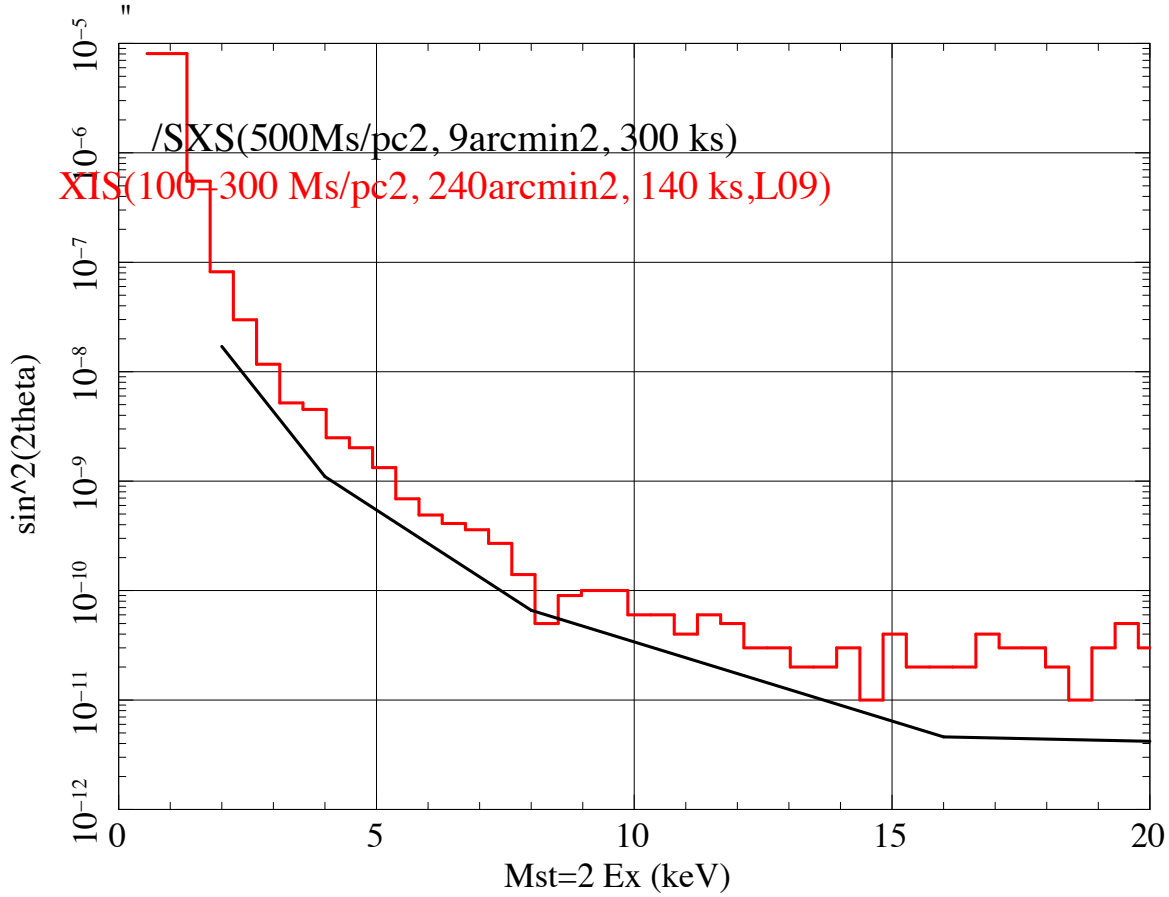

Limits on the decay rate with a SXS 300ksec of 500 $M_\odot/pc^2$ source (black). Red line shows the limit from Loewenstein+2009, where the dwarf galaxy Ursa Minor of *Suzaku* data of 100ks (XIS1) and 140 ks(XIS0+3) exposures were used.

Search for a weak and extended line at unknown energy: ASTRO-H/SXS or CCDs

- E< 1keV: The soft X-ray diffuse background dominates. Even for SXS, search for a weak line with this line dominated emission would be challenging.
- Some strong instrumental lines in CCD spectra (NXB). Limited energy resolution of CCD makes it difficult to search a line. SXS spectra could be much clean.
- Other bands:
  - Smaller extent source: SXS could be better, depending on DM distribution. Photon limit: T^{-1}.
  - Larger one: Large FOV CCDs could be better. Background limit $T^{-1/2}$
- If a line is detected: SXS can tell precise energy, making it easy to separate from non-DM origins. CCD detection is difficult to exclude non-DM possibilities.

What is best targets for X-ray dark matter search, a general consideration:

$M_{DM} = M_{tot} - M_{star} - M_{gas}$ Popular and bright astronomical sources are NOT good.

① **Dark matter massive sources** are essential. The source flux is proportional to Σ_{DM} and independent of the source distance, if the source is larger than the instrument's FOV.

② Toward the center, If density ↑ Σ_{DM} also ↑. In this case, **inner and dense regions** give higher Σ_{DM}. Nearby sources, where we can observe inner region, are better.

③ **Large Mtot/Mstar system** is better. Stellar mass dominated system (e.g. galaxy center) → the DM mass estimation uncertain.

④ **Large system** is better. DM mass is more robust in large integrated volumes. Small systems → local substructures or deviation from dynamical equilibrium. DM distribution smooth ?

⑤ **Large M_{tot} /L** system is better. found in small or large systems.

⑥ **X-ray faint source** is better. Dense and hot gas emits X-rays which is background for this study.

Ultra compact dwarf galaxies

Recently found by SDSS deep surveys

The most dark matter dominated system with M/L > 500-1000

But…

The Astronomical Journal, 142:128 (16pp), 2011 October doi:10.1088/0004-6256/142/4/128

WILLMAN 1—A PROBABLE DWARF GALAXY WITH AN IRREGULAR KINEMATIC DISTRIBUTION

Beth Willman[1], Marla Geha[2], Jay Strader[3,7], Louis E. Strigari[4],
Joshua D. Simon[5], Evan Kirby[6,8], Nhung Ho[2], and Alex Warres[1]
[1] Departments of Physics and Astronomy, Haverford College, Haverford, PA 19041, USA; bwillman@haverford.edu, awarres@haverford.edu
[2] Astronomy Department, Yale University, New Haven, CT 06520, USA; marla.geha@yale.edu
[3] Harvard-Smithsonian CfA, Cambridge, MA 02144, USA; jstrader@cfa.harvard.edu
[4] Kavli Institute for Particle Astrophysics and Cosmology, Stanford University, Stanford, CA 94305, USA; strigari@stanford.edu
[5] Observatories of the Carnegie Institution of Washington, Pasadena, CA 91101, USA; jsimon@obs.carnegiescience.edu
[6] California Institute of Technology, Pasadena, CA 91106, USA; enk@astro.caltech.edu
Received 2010 July 21; accepted 2011 July 30; published 2011 September 14

ABSTRACT

We investigate the kinematic properties and stellar population of the Galactic satellite Willman 1 (Wil 1) by combining Keck/DEIMOS spectroscopy with Kitt Peak National Observatory mosaic camera imaging. Wil 1, also known as SDSS J1049+5103, is a nearby, ultra-low luminosity Milky Way companion. This object lies in a region of size–luminosity space ($M_V \sim -2$ mag, $d \sim 38$ kpc, $r_{\rm half} \sim 20$ pc) also occupied by the Galactic satellites Boötes II and Segue 1 and 2, but no other known old stellar system. We use kinematic and color–magnitude criteria to identify 45 stars as possible members of Wil 1. With a systemic velocity of $v_{\rm helio} = -12.8 \pm 1.0$ km s^{-1}, Wil 1 stars have velocities similar to those of foreground Milky Way stars. Informed by Monte Carlo simulations, we identify 5 of the 45 candidate member stars as likely foreground contaminants, with a small number possibly remaining at faint apparent magnitudes. These contaminants could have mimicked a large velocity dispersion and abundance spread in previous work. The significant spread in the [Fe/H] of the highly likely Wil 1 red giant branch members ([Fe/H] $= -1.73 \pm 0.12$ and -2.65 ± 0.12) supports the scenario that Wil 1 is an ultra-low luminosity dwarf galaxy, or the remnants thereof, rather than a star cluster. However, Wil 1's innermost stars move with radial velocities offset by 8 km s^{-1} from its outer stars and have a velocity dispersion consistent with 0 km s^{-1}, suggesting that Wil 1 may not be in dynamical equilibrium. The combination of the foreground contamination and unusual kinematic distribution make it difficult to robustly determine the dark matter mass of Wil 1. As a result, X-ray or gamma-ray observations of Wil 1 that attempt to constrain models of particle dark matter using an equilibrium mass model are strongly affected by the systematics in the observations presented here. We conclude that, despite the unusual features in the Wil 1 kinematic distribution, evidence indicates that this object is, or at least once was, a dwarf galaxy.

Key words: galaxies: dwarf – galaxies: individual (Willman 1) – galaxies: kinematics and dynamics – galaxies: star clusters: general

Online-only material: color figures

Willman-I, Ultra compact dwarf galaxy

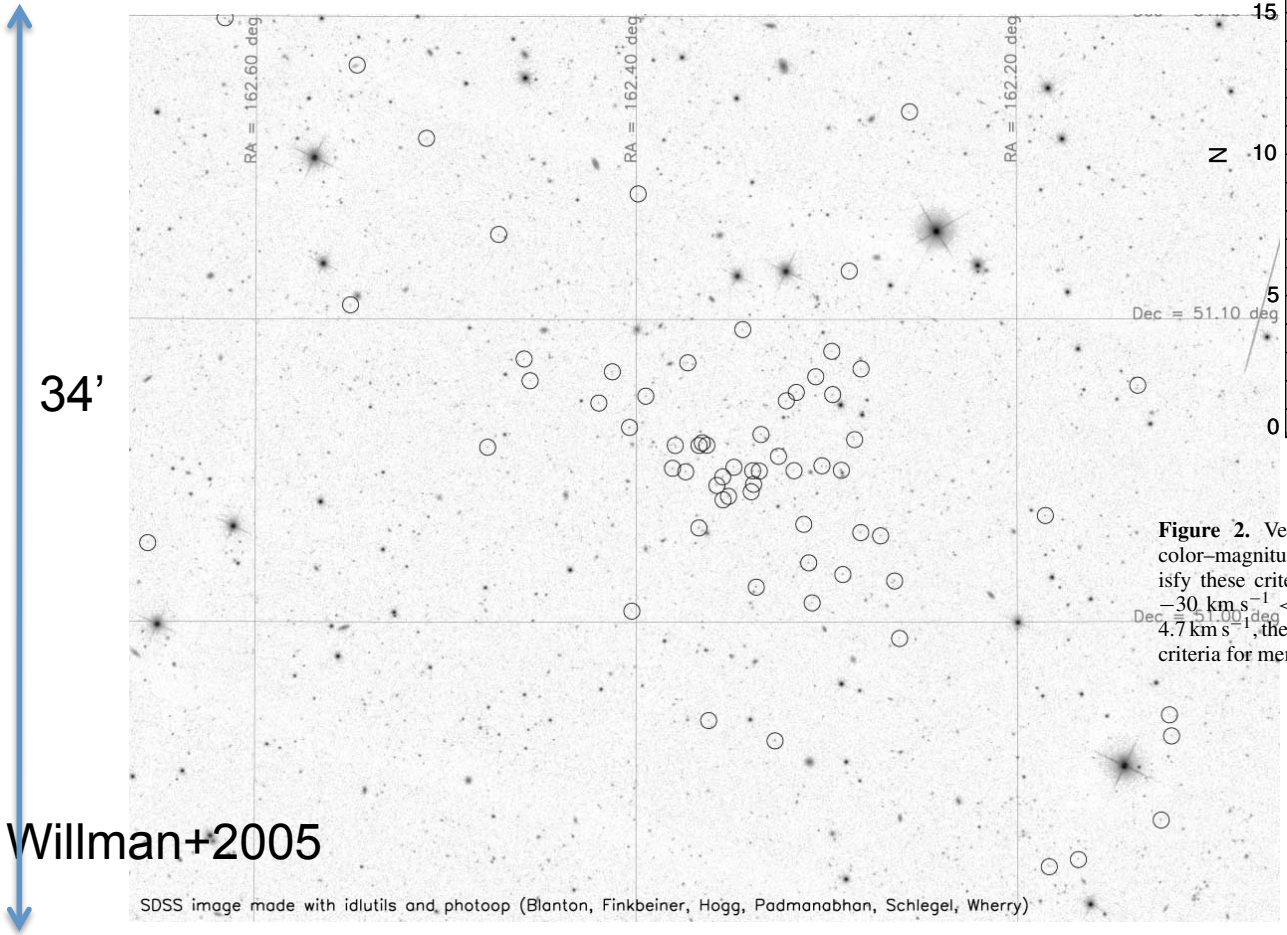

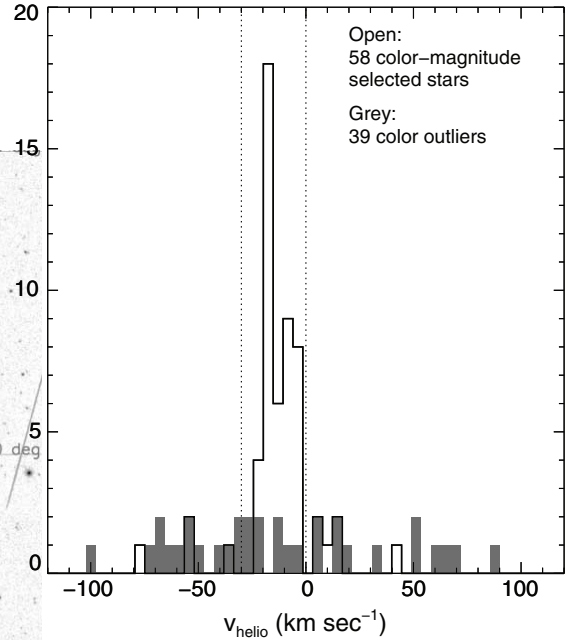

Figure 2. Velocity distributions of the 58 stars that satisfy our Wil 1 color–magnitude selection criteria (open) and the 39 stars that do not satisfy these criteria (gray filled). The dotted lines show the velocity range of $-30\ \mathrm{km\ s^{-1}} < v_{\mathrm{helio}} < 0\ \mathrm{km\ s^{-1}}$ used to select Wil 1 member stars. Binsize is $4.7\ \mathrm{km\ s^{-1}}$, the median velocity error of the 58 stars passing the color–magnitude criteria for membership.

FIG. 1.—SDSS true-color *g*, *r*, *i* image of $0.^{\circ}57 \times 0.^{\circ}42$ centered on the detection. Stellar sources with colors consistent with blue horizontal-branch and main-sequence turnoff stars ($g - r < 0.3$) are circled. The image is made with color-preserving nonlinear stretches (Lupton et al. 2004). [*See the electronic edition of the Journal for a color version of this figure.*]

Dark matter column density

Table 10: Mass distritbuion parameters. Cluster NFW parameters are taken from kT-M relation in Vikhlinin 2009. $r_s/R_{500} = 3$ is assumed for clusters. NFW parameters (r_s, ρ_s) for dwarf galaxies are taken from [Strigari et al.(2008b)] (Fig.1) and Strigari et al. 2007. Those of MW are from [Boyarsky et al.(2008)] and [Klypin et al.(2002)].

name	D_A (pc)	r_s (pc)	ρ_s ($M_\odot$ pc^{-3})	$r_s\rho_s$ ($M_\odot$ pc^{-2})	$1'$ (pc)
Perseus	7.50e+07	4.27e+05	1.00e-03	4.27e+02	2.18e+04
Coma	9.62e+07	4.90e+05	1.01e-03	4.95e+02	2.80e+04
Virgo	1.63e+07	2.53e+05	1.00e-03	2.53e+02	4.74e+03
Ursa-majorII	3.2e+04	6.0e+02	1.5e-01	9.0e+01	9.3e+00
Coma-Berenices	4.4e+04	3.0e+02	2.5e-01	7.5e+01	1.3e+01
Will-I	3.8e+04	2.0e+02	3.0e-01	6.0e+01	1.1e+01
Ursa-Minor	6.6e+04	1.5e+02	6.0e-01	9.0e+01	1.9e+01
Draco	8.0e+04	8.0e+02	6.0e-02	4.8e+01	2.3e+01
MW/Favoured	8.0e+03	2.2e+04	4.9e-03	1.1e+02	2.3e+00
MW/maximum-disk-A	8.0e+03	4.6e+04	6.0e-04	2.8e+01	2.3e+00
MW/maximum-disk-B	8.0e+03	2.3e+04	3.1e-03	7.1e+01	2.3e+00

Dark matter concentration (galaxy and cluster center) → Gas and stars concentrate → X-ray emission, absorption
Galaxy center → Dark matter has cusp or core ?

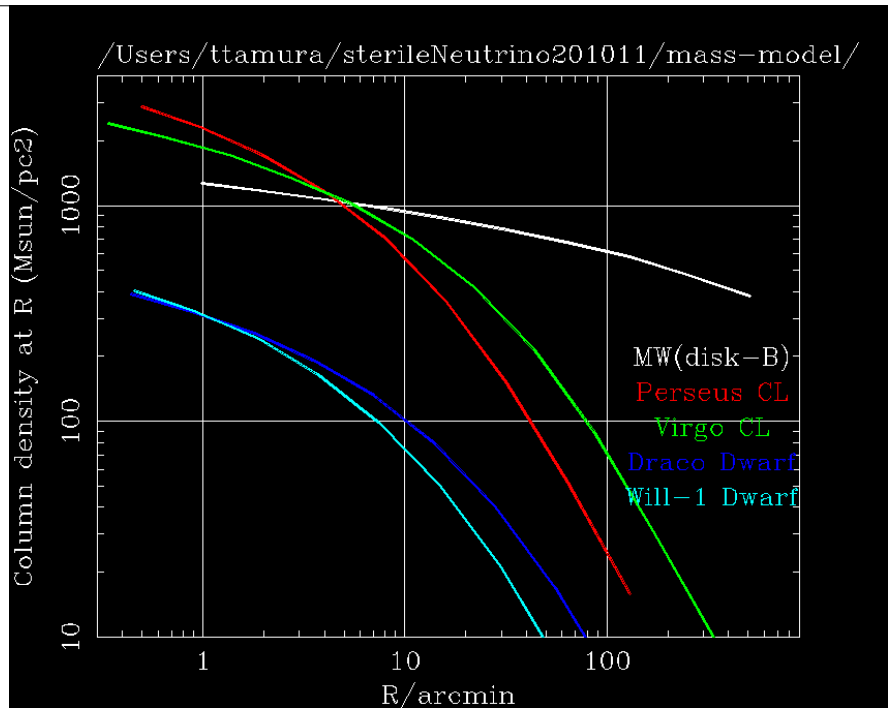

	(1) ΣDM ($M_\odot/pc^2$)	(2) DM estimate	(3) Size/ arcmin	(4) Lx/kT	(5)Note
1. Ultra compact dwarf	100-500	Cusp or core? Equilibrium ?	< 5	Very low	Mtot/L ~ 1000. New targets from future deep survey.
2. Classical dwarf	50-100	OK	>5	Very low	
3. Spiral G	50-150	OK at outer region	> SXS	Low (PS +ISM)	
4. Elli. G.	↑	↑	> SXS	Lines at < 1keV, PS	AH targets
5. Off-center of galaxies/Clusters	< 50	Substructure	> SXS	Low/bright	
6. MW/Andromeda core	> 500-1000	?, No DM	> SXS	Bright, usually	AH targets, Galactic absorption
7. Cluster core	> 500-1000	OK	< 3-5	Very bright	AH targets

The SXS simulation (1) The Perseus center

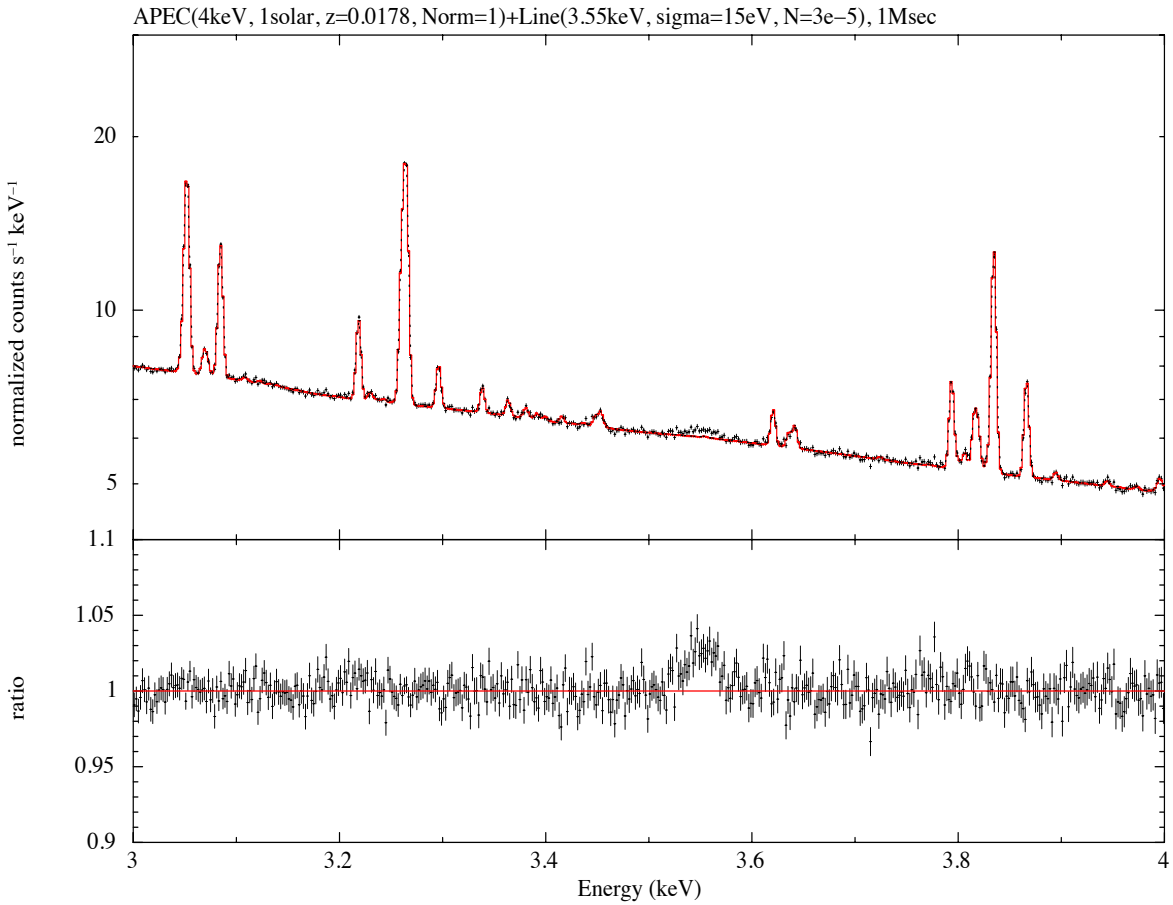

A simulation of 1Msec observation with a dark matter line at 3.55keV.
We assume a ICM thermal emission of kT=4keV, 0.7solar, z=0.0178, and a X-ray flux of the Perseus center. No turbulent line broadening is assumed. For the dark matter emission, line broadening of a FWHM of 35eV by σ=1300km/ velocity dispersion is assumed. Line flux is 3×10^{-5} ph/s/cm^2 (Bulbul+2014).The model in red assumes no DM line.

The SXS simulation spectra (1) dark galaxy

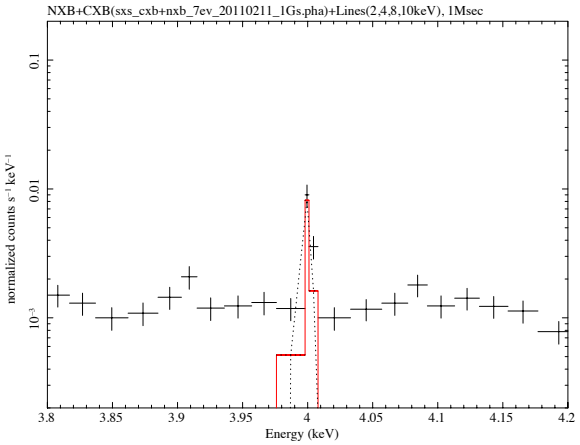

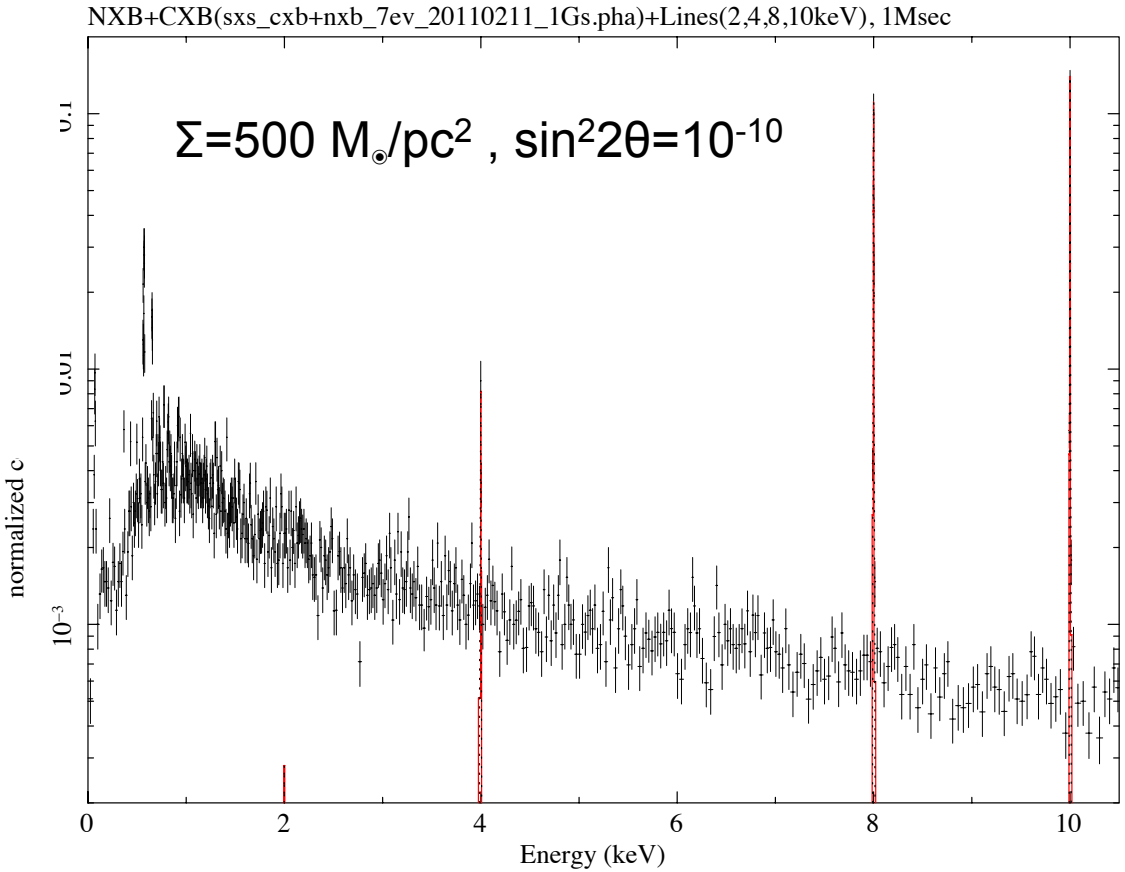

1 Msec of a galaxy without X-ray emission. Only estimated instrumental background is included. DM line at 2.0, 4.0, 8.0, and 10.0 keV are assumed. No line broadening due to the DM velocity is assumed.

Expected counts from dark matter with the *ASTRO-H* SXS

Table 9: Expected signal flux and count in *ASTRO-H* sxs. $\Sigma_{\rm DM}$ of 100 $M_\odot$ pc^{-2}is assumed. Above the line for each energy, $\sin^2(2\theta)$ is taken from a current limit in [Abazajian et al.(2007)].

DM-mass (keV)	X-ray (keV)	Area cm2	$\sin^2(2\theta)$	Flux (LU)	Flux (cts/s/cm2/sxs)	Rate (cts/s)	Rate (cts/1Msec)
1.0	0.5	40	1.0e-07	1.3e-02	9.9e-09	4.0e-07	4.0e-01
2.0	1.0	200	2.0e-08	4.2e-02	3.2e-08	6.3e-06	6.3e+00
4.0	2.0	250	1.0e-09	3.3e-02	2.5e-08	6.3e-06	6.3e+00
8.0	4.0	250	1.0e-10	5.3e-02	4.1e-08	1.0e-05	1.0e+01
10.0	5.0	250	4.0e-11	5.2e-02	4.0e-08	9.9e-06	9.9e+00
20.0	10.0	100	2.0e-12	4.2e-02	3.2e-08	3.2e-06	3.2e+00

A strategy for dark matter search with *ASTRO-H*

1. *XMM* and *Suzaku* show candidates of dark matter lines. In the early phase of the mission some objects (Clusters and Milky-way) with hints of un-id lines will be observed. High resolution clean and deep spectroscopy → separate the line from plasma or instrumental features.
2. Accurate line energy → identify lines in objects in various redshifts.
3. Line shape (width) → velocity dispersion of dark matter, different from those of metals in the plasma.
4. If a line was established, measure spatial distribution. Baryon X-ray $\propto n^2$, dark matter $\propto n$.
5. Dark matter massive but X-ray faint galaxies → higher S/N than X-ray bright clusters and galaxies. Better objects, to be discovered from recent large area surveys in optical and IR.
6. Stacking analysis of various regions compensate lower grasp (SΩ) of SXS.
7. Large Ω CCD (SXI) helps SXS.
8. New theory or motivation of dark matter X-ray are welcome to check.

Summary of the lecture

1. In the νMSM model, which aims to explain ν oscillations and baryon asymmetry, sterile neutrinos are introduced. Light sterile neutrino is a candidate of dark matter. Having a possible mass range of around keV, this decays into X-ray photons.
2. Because of an extremely low decay rate, this would be discovered exclusively from cosmic sources.
3. X-ray limit and DM mass assumption provide constraints on sterile neutrino parameters.
4. In 2014, two groups reported detection of an unidentified X-ray line from clusters and a galaxy at around 3.5 keV. *Suzaku* also suggested un-id lines from Galactic bulge.
5. In a search for the 3.5~keV line, we have used deep *Suzaku* spectra of the Perseus. We found no line so far.
6. Distinguishing a unidentified line feature from any atomic lines or instrumental effects is challenging, largely because of limited energy resolutions of current detectors (CCDs).
7. *ASTRO-H*, to be launched in 2015, is equipped with a X-ray calorimeter, as the prime instrument. This improves energy resolution at E>1.5 keV by a factor of > 20.
8. With deep *ASTRO-H* exposure, high energy resolution spectroscopy → resolve the unidentified X-ray line and separate from atomic or instrumental effects.
9. SXS spectra from clusters and the Galaxy → detect, separate, identify, and resolve lines. Central energy, spectral shapes, and spatial distributions are keys.
10. Dark matter massive but X-ray faint objects → Better chance of detection and constrains on dark matter parameters.